CHALMERS
UNIVERSITY OF TECHNOLOGY

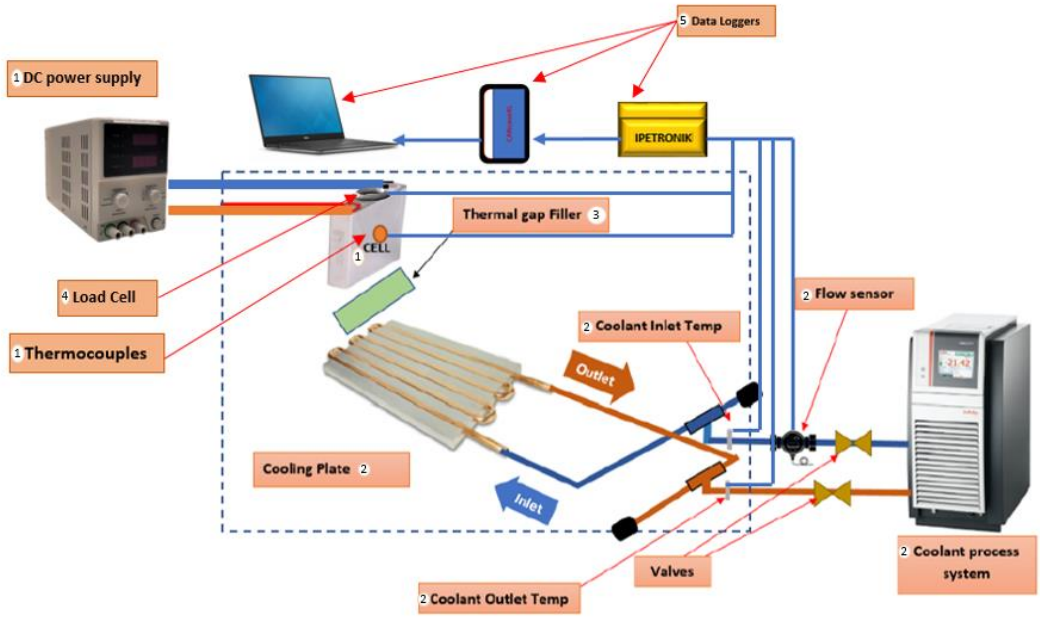

Investigation of the effects of Thermal Interface Materials on the Cooling of Battery Cells

A comparative study on the heat transfer properties

Master's thesis in Energy Storage Systems

Rohith Virinchi Maddila
Soroush Rostami

DEPARTMENT OF MECHANICS AND MARITIME SCIENCES
CHALMERS UNIVERSITY OF TECHNOLOGY
Gothenburg, Sweden 2023
www.chalmers.se

MASTER'S THESIS IN MECHANICS AND MARITIME SCIENCES

Investigation of the Effect of Thermal Interface Materials on the Cooling of Battery Cells

A comparative study on the heat transfer properties

Rohith Virinchi Maddila
Soroush Rostami

Department of Mechanics and Maritime Sciences
Division of Energy Conversion and Propulsion Systems
CHALMERS UNIVERSITY OF TECHNOLOGY
Göteborg, Sweden 2023

Investigation of the Effect of Thermal Interface Materials on the Cooling of Battery Cells
A comparative study on the heat transfer properties
Rohith Virinchi Maddila

Supervisor: Samani Marco, Volvo GTT
Examiner: Hua-Dong Yao, Division of Fluid Dynamics at the Department of Mechanics and Maritime Sciences at Chalmers University of Technology
Chalmers University of Technology
SE-412 96 Göteborg
Sweden
Telephone: + 46 (0)31-772 1000

Cover:
A schematic diagram of the experimental setup. See Figure 3.1

Investigation of the Effect of Thermal Interface Materials on the Cooling of Battery Cells
A comparative study on the heat transfer properties
Rohith Virinchi Maddila
Department of Mechanics and Maritime Sciences
Chalmers University of Technology

Abstract

The transport sector has been a significant contributor to the rising carbon footprint, primarily due to the use of fossil fuels as a power source. To mitigate this issue, the concept of electromobility has emerged, emphasizing electrically driven vehicles with batteries for various transportation modes. Enhancing battery efficiency is crucial for improving the performance of electric vehicles, achieved through an efficient Battery Thermal Management System (BTMS). The BTMS aims to optimize heat transfer from the battery, ensuring it functions within the operating temperature range. Among the effective BTMS approaches, the liquid cooling system stands out, aided by a Thermal Interface Material (TIM) placed between the batteries and the cooling plate. This master thesis, conducted in collaboration with ESS Component and Verification group in Electromobility at Volvo GTT, investigates the performance of commercially produced TIMs. Key parameters such as TIM thickness and applied pressure are altered to assess their impact on TIM performance.

This investigation employs a complementary approach of experimentation and simulation to study two different Thermal Interface Materials (TIMs): a thermal pad and a thermal gel. The focus of this thesis is on the thermal conductance of the TIMs, which is represented by a dummy cell maintained in a steady state of heating during the experimentation. The study begins by examining the thermal pad, with an emphasis on varying the applied pressure to evaluate its impact. Subsequently, a comparative study is conducted on the thermal gel, exploring the effects of both thickness and pressure on heat transfer through the TIM. The objective is to enhance heat dissipation and subsequently cool the battery. Through analysis and a review of existing literature, simulations were carried out to understand the effect of the thermal properties of these TIMs on the cooling of the batteries.

A comparative investigation was carried out using experimentation and simulations to examine the impact of varying the thickness of TIMs on the temperature of a simulated cell. The results indicated that when the TIM possessed a higher effective thermal conductance, achieved by increasing the pressure applied to it, the cell's temperature decreased. This outcome was consistent for both a 2 mm thermal pad and a 2 mm thermal gel. However, when the gel thickness was reduced to 0.5 mm, applying high pressure led to cracks inside of it which in turn led to a reduction in effective thermal conductance. The obtained results demonstrated that the highest pressure led to a 40% reduction in the thermal resistance for the 2 mm pad, while it was only a 16% reduction for the 2 mm gel.

Keywords: Heat transfer, BTMS, Dummy cell, TIM, Effective thermal conductance, Thermal resistance

Contents

Acknowledgments

It has been a pleasure for us to perform this master's thesis project. We would like to begin by extending gratitude to our supervisor Marco Majid Kabiri Samani and ESS component verification manager Hannes Kannisto at Volvo GTT who trusted us and gave us the opportunity to perform this thesis and strongly supported us throughout the process. This thesis wouldn't be complete without their involvement.

We would like to thank Ahmed Aijas from ESS system verification team and Rikard Hulthen who supported us during our experimentation process and has been a key member in helping us solve issues with the setup.

We would also like to thank Karlsson Stina and Dai Kaixiang from thermal simulation team who helped us with resources like the various thermal interface materials which have been tested in this thesis.

To add on, we would like to extend our thanks to Volvo Testing Technology that supported us with measurement tools and calibration techniques that have been an important part of this project.

Finally, a huge thank you to our examiner Huadong Yao at Chalmers who extended his knowledge on performing simulations that helped us avoid mistakes and finish this thesis on time.

Rohith Virinchi Maddila
Soroush Rostami, Gothenburg, June 2023

Nomenclature

EV	Electric Vehicles
HEV	Hybrid Electric Vehicles
PHEV	Plug-in Hybrid Electric Vehicles
ESS	Energy Storage Systems
BTMS	Battery Thermal Management System
PCM	Phase Changing Materials
TIM	Thermal Interface Materials
Q_{irr}	Irreversible heat generation [W]
R_{int}	Internal resistance [Ω]
I	Working current [Amps]
R_e	Reynolds no.
ρ	Density [kg/m^3]
L	Characteristic length [m]
V	Velocity [m/s]
μ	Dynamic viscosity [kg/ms]
C	Discharge capacity [1/h]
T	Temperature [K]
ΔT	Difference in temperature [K]
R_{TIM}	Thermal interface resistance [K/W]
Q	Heat flux [W]
$R_c = R_{c_1} = R_{c_2}$	Contact resistance at interface [K/W]
BLT	Bold Line Thickness [m]
λ_{TIM}	Thermal conductivity [W/mK]
LMA	Low Melting Alloys
P	Pressure [Pa]
LMTA	Low Melting Temperature Alloy
TCA	Thermal Conductive Adhesives
$\frac{\partial(\rho c_p T)}{\partial t}$	Accumulation term for energy [J]
$-V_j \frac{\partial(\rho c_p T)}{\partial x_j}$	Convective energy transfer [J]
$k \frac{\partial^2 T}{\partial x_j \, \partial x_j}$	Conductive energy transfer [J]
S_T	Energy from heat source [J]
q''	Heat flux in 3d form [W]
k	Effective heat transfer coefficient
$R_{th_{Al}}$	Thermal resistance of Aluminum [m^{2}K/W]
$R_{th_{si}}$	Thermal resistance of Silicon [K/W]
h	Thermal contact conductance [W/K]
h_s	Thermal contact conductance through solid [W/K]
h_g	Thermal contact conductance through inertial medium [W/K]
σ	Standard deviation
σ'	Combined standard deviation
F	Load applied [N]

A_a	Cross sectional area [m^2]
n	Load exponent
H	Microhardness [Pa]
DBC	CAN database file
λ_{eff}	Effective conductivity [W/mK]
BLT_{base}	Base thickness of TIM [m]

1 Introduction

Throughout history, the automotive sector has not prioritized sustainable methods. Conventional manufacturing processes, which are still widely employed today, consume substantial amounts of energy, metals, plastics, harmful substances, and labor, resulting in a substantial carbon footprint. Furthermore, after vehicles are manufactured, most of them rely on fossil fuels for operation, leading to the release of detrimental emissions. The overall process has had a profound environmental effect, culminating in our current situation.

Although COVID-19 has disrupted supply chains and car sales, it is crucial to recognize the industry's trajectory before the pandemic. According to a particular study, approximately 86 million cars were sold in a single year (2018), contributing to 9% of global greenhouse gas emissions [1]. This highlights the necessity for significant change and emphasizes the considerable positive impact that adopting sustainable practices in the automotive industry can have. Consequently, automobile manufacturers have shown significant interest in the advancement of electric vehicles (EVs) and hybrid electric vehicles (HEVs) [2]. Multiple types of EVs exist in the market which is being dominated by Battery Electric Vehicles (BEV) that have various levels of electrification and the plug-in HEVs (PHEV) that contain a bug enough battery to enable pure electric drive.

Volvo Group, as one of the biggest manufacturers of vehicles, is determined to contribute to driving their industry towards a sustainable future. Electromobility is a growing organization in place to shape the future in a way to have low emissions and fight against climate change. The electromobility department at Volvo Group develops and drives electrified products for trucks and buses as well as creates opportunities for all business areas. It is one of the fastest-growing departments in which Energy Storage Systems (ESS) play a key role within the electrified powertrain. At ESS, Volvo strives to develop world-class batteries for different applications, the focus of which is to maximize energy and power density. To enhance these parameters, Lithium-ion batteries tend to show a great prospect [3]. However, Lithium-ion batteries come along with a set of problems, one of which lies in the thermal management department which contributes to the loss in efficiency [3]. An effective solution to this problem can be found through the implementation of a battery thermal management system (BTMS). As a result, there has been a growing interest and research focus on BTMS in recent years.

The critical aspect of BTMS is to maintain the batteries in their operating temperature range in electric vehicles. There are three types of thermal management systems that are currently used in electric vehicles in the name of air-cooling systems, liquid cooling systems, and phase change materials (PCM) [4] the working principle of each is explained in Section 2.3.3. This project focuses on the effect of Thermal Interface Materials (TIMs) on the cooling of batteries using liquid cooling systems and the challenges encountered in improving the thermal efficiency of battery cooling. Currently, one of the main challenges with the usage of liquid cooling systems in regulating the temperature of the battery is the gap between the battery modules and the heat sink. Due to the irregular surface contact and the presence of air, between the batteries and the heat sink, the heat transfer process is inefficient. To solve this issue,

a TIM is placed between the coolant plate and the battery to promote the heat transfer process and thereby reduce the battery temperature, which is what this thesis is about.

1.1 Objective

This project focuses on the comparative analysis of the performance of the Thermal Interface Materials with different thicknesses, placed between the battery and the coolant plate when different pressures are applied to the battery. This is done to understand the effect of thickness and pressure on the thermal resistance between the battery and the cooling plate.

2 Theory

This section of the thesis project covers the underlying principles related to the research, including the prior investigations and preliminary examination. The chapter begins with a summary of Lithium-Ion batteries, with an emphasis on their functionality and concerns regarding thermal regulation. The next section discusses techniques for enhancing thermal management, particularly through the use of liquid cooling systems and the optimization using thermal interface materials (TIM). The last section provides a thorough explanation of the TIM's heat transfer characteristics and the various factors that impact its thermal conductance.

2.1 Li-Ion batteries

2.1.1 Why Li?

Lithium is the lightest metal and has a low electrochemical potential, making it highly reactive. Its small radius allows it to be used in various insertion host materials, making it suitable for use in electrochemical cells with high-energy and power densities. The lithium battery is a type of rechargeable battery that uses lithium ions as charge carriers and has a cell potential typically ranging from 2.5 V to 4.5 V.

The family of lithium batteries varies widely in terms of chemistry, performance, and safety characteristics, and can be optimized for specific requirements. The lithium-ion battery, which is part of this family, is the most common rechargeable battery used in portable electronics and electric vehicles with an all-electric driving range. By using different materials for the electrodes and electrolytes, lithium-based cells can be customized for specific applications, including capacity, rate, high-energy, and power density. These cells are generally lightweight with a high open circuit voltage, resulting in a positive impact on energy density. They can be cycled over a wide state of charge range, and some basic chemistries allow for constant cell voltage over a wide range. Fast charging is possible, and the shelf life is acceptable.

Maintaining temperature control is important for most lithium battery designs, primarily due to the electrolyte's instability, which may lead to side reactions resulting in capacity loss or thermal runaway. Overcharging the cell may also cause the same effects. To mitigate these risks, lithium batteries must have a management unit with a protective circuit that regulates temperature, currents, and voltage levels. This unit will shut down the battery if an abusive situation arises. At low temperatures, even at 10°C in some cases, charging lithium batteries may cause side reactions and rapid degradation due to increased internal resistance.

In the basic layout of the lithium battery, the two electrodes are materials allowing lithium ions to be inserted/extracted according to:

$$Host + Li^{+} + e^{-} \leftrightarrow Li - Host \qquad 2.1$$

The host structures and materials used in different types of lithium batteries vary, with some combinations being more suitable for hybrid electric vehicles and others for electric vehicles. Water-based electrolytes cannot be used due to the high cell voltage

which is why non-aqueous electrolytes are used instead. These can take the form of a liquid, solid polymer, or gel, with a dissolved lithium salt. The most used lithium battery concepts are lithium metal, lithium-ion, and lithium-ion polymer. Recently, there has been renewed interest in two other lithium-based battery concepts: lithium-oxygen and lithium-sulfur batteries.

2.1.2 Working of Li-ion battery

A lithium-ion battery operates based on electrochemistry principles. It has a cell composed of a cathode, an anode, a separator, an electrolyte, a positive current collector, and a negative current collector. The electrolyte carries charged lithium ions back and forth between the anode and cathode where they are stored. This movement creates free electrons, which induce a charge at the positive current collector, causing an electrical current to flow through the powered device and back to the negative current collector. The separator prevents electrons from flowing within the battery cell. Lithium-ion batteries come in different types with varying combinations of materials used for the electrodes, cathodes, anodes, and electrolytes.

The redox reactions that undergo during the charging and discharging processes are given by:

While charging,

$$\textit{Anode: } LiCoO_2 \leftrightarrow Li_{(1-x)}CoO_2 + xLi^+ + xe^- \qquad 2.2$$

$$\textit{Cathode: } 6C + xLi^+ + xe^- \leftrightarrow Li_xC_6 \qquad 2.3$$

While discharging,

$$\textit{Anode: } Li_{(1-x)}CoO_2 + xLi^+ + xe^- \leftrightarrow LiCoO_2 \qquad 2.4$$

$$\textit{Cathode: } Li_xC_6 \leftrightarrow 6C + xLi^+ + xe^- \qquad 2.5$$

Battery cells can have various designs, but in-vehicle applications, the two common ones are prismatic and cylindrical cells, each with unique benefits. Cylindrical cells are more mature in terms of production; hence they are cheaper to manufacture. On the other hand, prismatic cells, which are being studied in this project, offer better space utilization and versatality compared to other designs. The prismatic cell resembles a flat bag that has been compressed to form a rectangular shape. As a result, the prismatic cell exhibits anisotropic heat transfer, with greater thermal resistance on the flattened side [5].

2.2 Thermal management of Li-ion batteries

The Battery Thermal Management System (BTMS) takes into consideration several parameters linked to each other and most of the parameters are path dependent. Each of these parameters has an influence on the battery control and management system, which are, temperature, voltage range and current input. In this report we will be stressing only on the temperature influence, its effects on the performance of the cell and how can it be controlled. It is of a known fact that for the battery to give its best performance, the temperature of the cell must be maintained in its operating range of +20℃ to +40℃ [6]. Not just the temperature of each cell but the temperature differences among the cells should also be held at a minimum.

It's likely that temperature differences will be present in a battery, resulting in variations in the performance and aging rates of the cells depending on their position within the battery. Although a well-designed battery can minimize these temperature differences, they cannot be eliminated which also affects cell balancing. Higher temperatures lead to better cell performance due to faster cell reactions, which enables higher power output and reduces impedance, thereby increasing cell capacity [4]. However, temperatures outside the optimal range can lead to irreversible side reactions, resulting in increased aging rates. Therefore, there is an upper-temperature limit for optimal battery operation and durability. The same applies to low temperatures, where the battery's performance can significantly decline, and low-temperature operation can cause severe damage to the battery [7]. The BTMS should ideally maintain the temperature in a pre-defined zone and detect unexpected temperature changes. The temperature and voltage relationships in terms of safety ranges is shown in the Figure 2.1, the ideal operating temperature being +20℃ to +40℃.

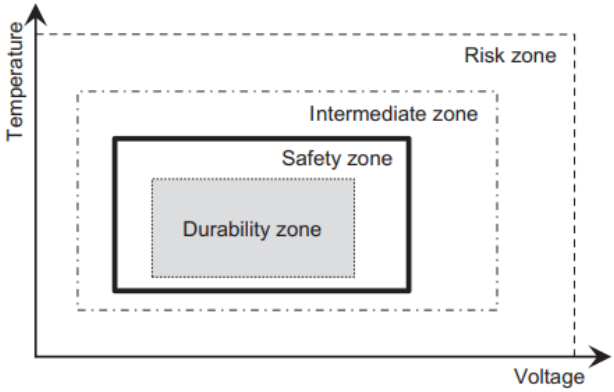

Figure 2.1: Schematic voltage and temperature safety ranges [7]

2.2.1 Sources of heat inside the battery

The nature of cell reactions in batteries means that any battery operation will produce heat, along with heat generated by resistance within the cell during charging and discharging processes. Three main sources of heat generation within the cell are activation losses due to interfacial kinetics, concentration losses due to species transport, and ohmic losses caused by charged particle movement. Overpotentials cause activation losses, while Joule heating is often the result of ohmic losses, causing temperatures to rise to around 60-80 degrees Celsius. Heat generation due to overpotentials varies during charging and discharging, so heat transfer varies as well.

Battery heat generation is transient, depending on the state of charge, and it increases as the battery reaches the end of charging and discharging. The thermal behavior of a battery may differ depending on the technology used. In this report, we will be focusing on the consequences of Joule heating and how do we reduce its impact on the performance of the battery.

In lithium-ion batteries, joule heating occurs when an electric current is passed through the electrodes and electrolyte. During charging and discharging, ions move between the electrodes through the electrolyte, which generates a flow of electrons in the external circuit [4]. This flow of electrons encounters resistance in the battery's materials, resulting in the generation of heat. The heat generated, resulting in a decrease in battery capacity and power due to the loss of lithium and active materials within the battery, can be described as irreversible losses, as stated by,

$$Q_{irr} = R_{int} \cdot I^2 \qquad 2.6$$

Where Q_{irr} is the irreversible heat generation, R_{int} is the internal resistance, and 'I' refers to the working current in the cell. The flow of electricity in the battery is influenced by the pattern of usage, and it rises when more energy is either being drawn out or put into the battery, like during intense acceleration or rapid charging. Because the amount of heat produced is proportional to the square of the current flowing, the impact of high-power usage results in a significant increase in heat production. When the BTMS is not working well, the rise in power consumption results in a rise in battery temperature.

This can lead to several undesirable effects which can increase the rate of chemical reactions within the battery and accelerate degradation of the electrodes and electrolyte. Additionally, if the heat generated is not dissipated efficiently, it can cause localized temperature increases, which can result in thermal runaway and even catastrophic failure of the battery [8].

2.2.2 Types of BTMS

At present scenario, there are multiple types of BTMS in use that are separated into three main categories based on the coolant and its phase [6]. The first being the air-cooled system in which the coolant is air and remains in the gaseous phase. The second category is liquid coolant systems in which the coolant is in liquid phase. Finally, phase change materials (PCM) that absorb heat and change its phase. The following sections briefly describe each of these categories:

Air cooling system

Air-cooled systems can be divided into two categories: active and passive. Passive systems utilize natural convection and heat dissipation through a heat sink, and they have low cost and weight because they require only a few additional components. Active systems, on the other hand, use a fan or blower to increase heat transfer, resulting in a higher cooling rate but also higher complexity and cost [9]. Air-cooling structures can be of different types, with the most common being series and parallel cooling structures [10]. The design of the flow channels is an important factor in the performance of air-cooling systems, with various design solutions proposed by researchers. One popular design is a double U-type duct for cooling the battery from a

bottom plate [11]. Ventilation channels can be designed in series or parallel, with parallel structures achieving lower temperature and more uniform temperature distribution [10]. [12]Another improvement is to use aluminum foam in the air channels to increase the heat transfer surface, which can reduce driving costs but also increase investment costs. To sum it up, air-cooled system in electric vehicles is limited due poor efficiency. Although, they are better in terms of simplified structure, low cost, and low maintenance [13]. Aside from the advantages of possible low weight and cost, these systems are also capable to work at low ambient temperatures [14].

Liquid cooling systems

Due to their higher thermal conductivity compared to air, liquids are preferred as coolants. Liquid cooling systems can be categorized as direct or indirect. In a direct cooling system, the liquid directly comes in contact with the battery, which limits the coolant options to prevent any potential hazards. On the other hand, an indirect cooling system has fewer restrictions on the choice of coolant since the fluid is separated from the battery. However, due to the contained coolant in indirect cooling, it has a higher thermal resistance in comparison to direct liquid cooling. Despite this, indirect cooling is still the more commonly used system in-vehicle applications [5]. Selecting the appropriate coolant is a critical factor for the performance of the liquid cooling system, where typical options include water, glycol, oil, acetone, and refrigerants [9]. The choice of coolant depends on the working environment and freezing point is a significant consideration. Additionally, fluid properties such as viscosity, density, and velocity affect turbulence and pressure drop, which can impact the efficiency of the liquid BTMS. The equation 2.7 following this statement demonstrates the relationship between turbulence and fluid properties.

$$R_e = \frac{\rho V L}{\mu} \qquad 2.7$$

Where ρ is the density of the fluid, V is the velocity, L is the characteristic length scale and μ is the viscosity of the fluid. The pressure drop in the system is affected by the same factors that impact turbulence. An increase in turbulence can result in an increase in pressure drop and the need for more pump work. To improve the cooling performance and ensure a better consistent battery temperature, nanoparticles can be added to the coolant [15]. Another method to enhance heat transfer is by increasing the surface area for heat exchange, which can be achieved by implementing fins on either the fluid side or in contact with the cells [16]. Compared to indirect cooling systems, direct liquid cooling systems, which involve submerging battery cells in a coolant, have the potential to provide improved heat transfer. This is attributed to reduced thermal resistance and increased contact surface area [17].

Direct liquid cooling systems can have a design similar to air-cooled systems, such as a system that uses silicon oil instead of air to improve cooling efficiency. Direct cooling solutions have mainly been studied for cylindrical cells and typically use electric insulating coolants, although some research has explored the use of liquid metals, which have shown promising results [18]. However, more research is needed before direct cooling can be commercialized, particularly in areas such as the

viscosity of the cooling media, the stability of the coolant for safety reasons, and the sealing properties of the system [19].

In vehicle applications, indirect liquid cooling is generally considered the better choice, and comparative studies have shown that direct cooling and air-cooling are less practical and efficient. In the case of indirect liquid cooling systems, a typical design includes a cooling plate positioned between the battery cells, modules, or packs. The efficiency and intricacy of the system tend to increase as the cooling plate is positioned deeper within the battery structure.

This passage discusses the design and optimization of cooling plates for indirect liquid cooling systems in vehicle battery packs. The physical design of the cooling plate channels including the material, mass flow rate, flow direction, and entrance size can all influence the cooling performance. Experimental studies involving mini channels have demonstrated a noteworthy reduction in the maximum temperature. Furthermore, research has indicated that increasing the coolant flow rate leads to a decrease in temperature variance [20]. Nevertheless, it should be noted that there exists an optimal flow rate beyond which the impact of further increasing the flow rate becomes less pronounced. Additionally, a higher flow rate results in a significant increase in the energy required by the pump [21]. A study showed that by increasing the flow rate from 1 l/min to 4 l/min, the pump work increased nearly 47 times [22]. Due to the increase in the work done by the pump, balance optimization of the flow rate is needed to be done. Achieving the ideal flow rate requires finding a balance between effective cooling performance and minimizing pressure drop. Further improvements in design can be made by introducing flexible graphite material between the channels and battery cells. This addition enhances cooling performance by ensuring a more uniform distribution of cooling. Additionally, optimizing the pattern of the cooling plate can contribute to achieving even temperature distribution, minimizing pressure drop, and lowering the average temperature.

Tesla has developed a solution for cylindrical cells where aluminum tubes covered in a dielectric material are bent around the cells, and this was implemented with a counterflow using a water-glycol mixture as coolant [23]. The hydraulic diameter of the cooling channel has no influence on either the maximum cell temperature or the temperature uniformity, but it should be adjusted to limit the pressure drop [24].

Liquid cooling systems are the current best solutions for cooling vehicle battery packs, but they have drawbacks such as potential coolant leakage, weight, and high complexity [19] [5] [25]. Research in air-cooled systems for vehicle applications has increased in interest, but there are several challenges to overcome for larger installations. Overall, it is of the shared opinion by several major car manufacturers that liquid cooling systems are favored as efficient BTMSs today [25].

Phase changing materials (PCM)

Phase-changing materials offer a passive cooling approach, in which the material absorbs or releases significant amounts of energy over a narrow temperature range as it transitions between phases, such as from solid to liquid or vice-versa. Since battery heat flux varies based on the driving cycle, cooling demands are not constant. PCM has demonstrated superior performance over other BTMS in managing sudden temperature spikes during high-power usage, as it can absorb or release heat until the

phase change is complete [26]. However, there is a risk of temperature run-off after the PCM completes the phase change and stops absorbing heat, so complementary cooling systems, such as air or liquid cooling, are necessary to cool the PCM and avoid heat accumulation. By combining PCM with complementary BTMS, the cooling system's weight, space, and cost can be reduced, and sudden temperature spikes can be addressed quickly [27]. The primary advantages of PCM are the reduced need for large equipment and the fast feedback on temperature spikes. PCM typically refers to the phase change between liquid and solid, but phase changes between liquid and gas have also been investigated, such as boiling fluids in microchannels. A direct boiling system has been demonstrated to maintain a battery package of prismatic cells at a constant temperature of 35°C, even under high discharge rates of up to 20C, with a temperature variance over the cell of only 4K [28]. The boiling temperature can be adjusted with pressure and working fluid, making direct PCM an efficient option. However, the optimal performance of a boiling system depends on the battery's heat generation, and various working fluids and orientation designs have been tested [29].

Efficient heat transfer relies heavily on the contact surface, making flattened pipes more favorable over circular ones. Thermal grease is commonly used as a thermal interface material to reduce contact resistance [4]. Similar to liquid cooling systems, nanoparticles can be added to the working fluid in pipe applications to increase heat transfer efficiency [30]. Passive PCM systems offer several practical advantages, including simplicity, lightness, high efficiency, and smaller components, making them suitable for vehicle applications. However, the poor thermal conductivity within PCM presents a major challenge, leading to a high risk of thermal run-away once the phase change is complete. The use of conductive fillers in thermal interface materials, along with embedding phase change materials (PCM) in porous materials or metal meshes, can enhance thermal conductance and mitigate the risk of PCM leakage by utilizing capillary forces to bind the liquid PCM. However, one potential issue with these approaches is that they may not always provide electrical isolation. This lack of electrical isolation can pose challenges in certain applications where electrical insulation is required to prevent any unwanted electrical conductivity or short circuits [4]. The potential of PCM is debated, with some tests showing as low performance as air-cooling, but with higher costs and complexity [31]. The implementation of PCM may not necessarily reduce weight, space requirements, or costs due to its complexity and need for additional cooling.

2.3 Thermal interface materials (TIMs)

2.3.1 What is a TIM?

A Thermal Interface Material (TIM) is a material that is used to improve the heat transfer properties between two surfaces. As described in Section 2.2.2 battery cooling systems are designed to manage the heat generated by the battery during normal operations in which the primary methods include air cooling, liquid cooling and PCM cooling. While TIM can be used in these cooling systems to improve heat transfer between the battery and cooling plate, it is not typically considered the primary source of cooling batteries. Rather, it is often used to enhance the performance of other cooling methods, such as liquid cooling or phase cooling.

2.3.2 Why is a TIM used?

The main challenge encountered during the usage of liquid cooling systems in BEVs is the gap between the heat source and the heat sink. Since air is a bad conductor of heat, there is a higher thermal resistance which leads to a higher temperature drop between them. To prevent this problem, a TIM is introduced between the source and the sink that reduces the thermal resistance and promotes the conduction of heat. This reduces the temperature drop as shown in the Figure 2.2

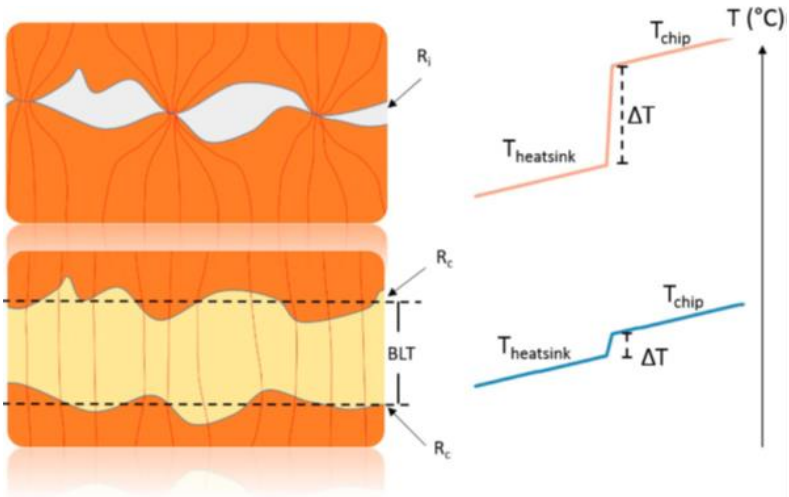

Figure 2.2: Working Principle of the Thermal Interface Material (TIM) [2]

The thermal performance of the TIM is evaluated by thermal interface resistance which is a variable that measures how difficult it is for the heat to cross the interface. This variable is calculated by heat flux across the interface and the temperature drop over it.

$$\Delta T = R_{TIM} \cdot Q \qquad 2.8$$

In the equation, ΔT is the temperature drop over the interface, Q is the heat flux and R_{TIM} is the thermal resistance. The idea is to reduce the thermal interface resistance which can be written as the sum of the three resistive components:

$$R_{TIM} = R_{c_1} + \frac{BLT}{\lambda_{TIM}} + R_{c_2} \qquad 2.9$$

Where R_{TIM} is the total thermal interface resistance, R_{C1} and R_{C2} are the contact resistances at the interface between the TIM and the two surfaces in contact with TIM. λ_{TIM} is the thermal conductivity of the TIM and BLT is the Bold Line Thickness of the TIM [32]. To minimize the R_{TIM} there are three factors to consider: thermal contact resistance (R_{C1} and R_{C2}), TIM thickness (BLT), and thermal conductivity of the TIM (λ_{TIM}) as explained below:

Thermal contact resistance: $R_{C1}$and R_{C2} depend on how well the TIM confirms the surface and fills out the voids. The contact resistance can be highly dependent on the pressure applied to the TIM.

TIM thickness: As it is presented the equation 2.9 lower the thickness applied, lower the thermal interface resistance is achieved. However, in practice decreasing the thickness of the TIM can lead to voiding and increasing the thermal contact resistance due to uneven coverage.

TIM thermal conductivity: The thermal conductivity of the TIM is the measure of how well the material conducts heat. The importance of high thermal conductivity is dependent on the thickness of the TIM. In the very low thickness, the contact resistance dominates the thermal interface resistance but in the high-thickness thermal conductivity of the TIM becomes much more important.

2.3.3 Types of TIM

There are various types of TIM available in the market currently including thermal greases, phase-changing materials, and carbon-based materials. Based on the scope of this project, this report will be showcasing deep into thermal pads, greases, and thermal gels but not so much about carbon-based materials:

- **Thermal grease**

Thermal greases are composed of a polymer base blended with ceramic or metallic fillers. Silicone is often chosen as the base material for thermal greases due to its thermal stability, wetting properties, and low elasticity. Ceramic fillers, including alumina, aluminum nitride, zinc oxide, silicon dioxide, and beryllium oxides, are commonly used in thermal greases. Additionally, metallic fillers like silver and aluminum are also employed in the formulation of these greases. To create a thermal grease, these components are combined to form a paste that can be applied to mating surfaces. When the grease is used on rough surfaces that are pressed together, it fills in the gaps and eliminates trapped air. The thermal conductivity of the thermal grease typically improves with a higher loading, meaning a higher fraction of fillers. However, this is also affected by the viscosity and wettability of the polymer used. The particle size is another important factor as it can act as spacers between surfaces, influencing the thickness of the bond line and subsequently the thermal resistance.

Research has indicated that achieving an optimized distribution of particle sizes can lead to a lower-viscosity material that is easier to handle during processing. Mixing particles of different sizes has been found to result in lower viscosity compared to using the same volume fraction of particles that are all the same size.

A drawback of using thermal grease is the potential for excessive grease to escape from the joint region and affect surrounding components. Although thermal greases effectively reduce heat resistance between flat surfaces, they do not offer electrical insulation between the surfaces. Furthermore, over time, power cycling and the natural expansion/contraction of components can cause the thermal grease to migrate and dry out, resulting in a loss of an effective thermal conduction path. To maintain the integrity of the joint, mechanical hardware is necessary. The failure mechanisms of thermal greases are closely tied to the temperature of the device and the frequency of on/off cycles it undergoes. As temperature increases, the pump-out [33] and phase separation effects also increase, leading to a twofold increase in degradation for every 10°C increase [34] in the operating temperature of the TIM. Power cycling between 0

and 100°C over 7500 cycles can cause a 4-to-6-fold increase in thermal resistance, while cycling between 0 and 80°C over 2500 cycles leads to negligible rise in resistance [34].

Khatri et al. [35] have developed a new type of thermal interface material called MicroFaze® which is a non-silicone thermal grease. Unlike traditional silicone-based products, MicroFaze® is dry to the touch and can solve contamination and migration problems. The product is composed of a substrate made of either aluminum or Kapton material, which is coated on both sides with non-silicone thermal grease. The thermal grease has a naturally tacky texture but feels dry to the touch. Unlike wax-based alternatives, this product offers thermal conductivities ranging from 0.9 to 5 W/mK and a thermal resistance of 0.13 to 0.2 ℃cm^2/W These properties are comparable to those of modern grease products, but without the drawbacks mentioned earlier.

- **Thermal Pads**

Thermal pads, like thermal grease, contain thermally conductive materials mixed in a polymer matrix. However, thermal pads use a heavily crosslinked polymer matrix, resulting in a solid pad that is easier to work with. This solid pad has some drawbacks, such as being thicker (around 200-1000 μm) [34] and requiring high pressure to conform properly to substrates. The pad's softness is crucial for it to conform to the substrate, but higher filler fractions of conducting particles make the composite stiffer, limiting its overall performance due to the trade-off between softness and filler fraction.

- **Thermally conductive elastomers (gels)**

Thermally conductive elastomers typically consist of a silicone elastomer base mixed with thermally conductive ceramic particles. They may also incorporate woven glass fiber or dielectric film to enhance mechanical strength. These elastomers are commonly employed in applications that demand electrical isolation. Unlike thermal grease, which has a flowing consistency, elastomeric TIMs require compressive pressure to conform to surface irregularities and establish effective thermal contact. At lower pressures, the elastomer may not adequately fill the gaps between surfaces, leading to increased thermal interface resistance. However, as the pressure is increased, the elastomer fills more of the microscopic voids, leading to a reduction in thermal resistance. To ensure the stability of the joint once it is assembled, a permanent mechanical fastener is necessary. The thermal resistance achieved depends on factors such as the thickness of the elastomer material, the applied clamping pressure, and the bulk thermal conductivity of the material.

- **Thermal conductive adhesives (TCAs)**

TCAs can create connections between substrates without requiring external pressure or fastening. TCAs, like TIMs, contain a thermally conductive substance mixed into a polymer matrix, usually epoxy. These substances are typically dispensed as liquids and solidify as they cure, creating a strong bond. While TCAs and gels share some similarities, TCAs are generally more inflexible and have stronger adhesion properties between substrates. There are also solid versions of TCAs that can be used like double-sided tape.

2.3.4 Factors affecting the selection of TIM

When choosing a thermal interface material, various factors must be considered. These factors include the performance of the TIM for a specific application, its reliability, and the installation process. The following are some typical features of a TIM that can impact the selection process:

Thermal Conductivity: The thermal conductivity of a thermal interface material plays a crucial role in its ability to transfer heat across the interface, thereby affecting its overall thermal performance.

Thermal Resistance: As defined in section 2.3.2 the thermal resistance should be ideally as low as possible to maintain the battery temperature in its operating range.

Electrical Conductivity: While some thermal interface materials possess electrical conductivity, they are typically composed of polymers or polymer blends containing non-conductive substances, so that electrical conduction is not a concern.

Phase Change Temperature: The phase change temperature of a thermal interface material refers to the temperature at which it transitions from a solid to a liquid state, filling any gaps and removing any trapped air. It's important to ensure that the melting temperature is lower than the maximum operating temperature of the device, so that the material can efficiently transfer heat across the interface. Additionally, it is crucial for the thermal resistance of the material to be as high as possible to prevent premature phase change during transportation. Research conducted by Bergquist indicates that temperatures as high as 60°C can be experienced during shipping. Therefore, the thermal interface material should possess sufficient thermal resistance to withstand these elevated temperatures and maintain its stability throughout the transportation process.

Viscosity: The viscosity of a phase change material above its phase change temperature must be sufficient to prevent the thermal interface material from flowing when it is oriented vertically. If the viscosity is too low, there is a risk of the TIM dripping or draining out of the assembly.

Operating Temperature Range: The suitability of a TIM is based on its operating environment. Certain TIMs have a narrow operating range. For instance, thermal pads have a wider range compared to thermal gels as pads are often made of materials with higher thermal conductivity.

Pressure: The application of TIMs is influenced by the amount of pressure applied during installation. Applying an appropriate amount of pressure can help to improve the performance of the TIM by reducing the thickness of any air gaps or voids that might exist between the two surfaces being joined. This allows for better thermal conductivity and heat transfer across the interface.

Thickness: In the context of TIMs, the thickness of the TIM directly affects its resistance to heat transfer. Thinner TIMs exhibit greater heat transfer efficiency compared to thicker ones because they offer a shorter path for heat to traverse. Therefore, reducing the thickness of the TIM can enhance the overall thermal performance of the system by minimizing the thermal resistance and facilitating more efficient heat dissipation.

Outgassing: The release of volatile gases when materials are exposed to high temperatures and/or low atmospheric pressures is known as outgassing. Most polymers, such as elastomers and silicones, will outgas to some extent which can be particularly concerning in aerospace applications, where outgassing is accelerated due to reduced pressures, and it may also cause issues within sealed cavity packages.

Surface Finish: The ability of TIMs to fill large gaps in irregular surfaces can vary depending on the specific product and the type of filler particles used. The interaction between the filler particles and the microscopic projections on the adjoining surfaces can influence the level of compaction and wetting at the interfaces. Some TIMs may be better suited for filling large gaps and conforming to irregular surfaces than others, depending on their material properties and filler particle characteristics.

Long-term stability and reliability: Thermal interface materials (TIMs) are expected to maintain consistent performance throughout the lifespan of the electronic device they are used in. The lifespan of electronic devices, such as microprocessors, is typically designed to last for seven to ten years. However, avionics and telecommunication devices are expected to survive for decades, which places additional demands on the reliability and consistency of the TIMs used in these applications.

The scope of this project is to focus only on the effect of thickness and pressure on the thermal conductive properties of a TIM and hence will be elaborating on the mentioned factors.

2.4 Heat transfer

In this chapter, the heat transfer equations that have been used in this project are going to be presented. Heat can be transferred through three models: Conduction, Radiation, and Convection which are demonstrated in Figure 2.3. This study disregards radiation due to the small variation between the temperature of the battery and the surrounding environment. Additionally, convection heat transfer is also ignored due to the presence of insulation.

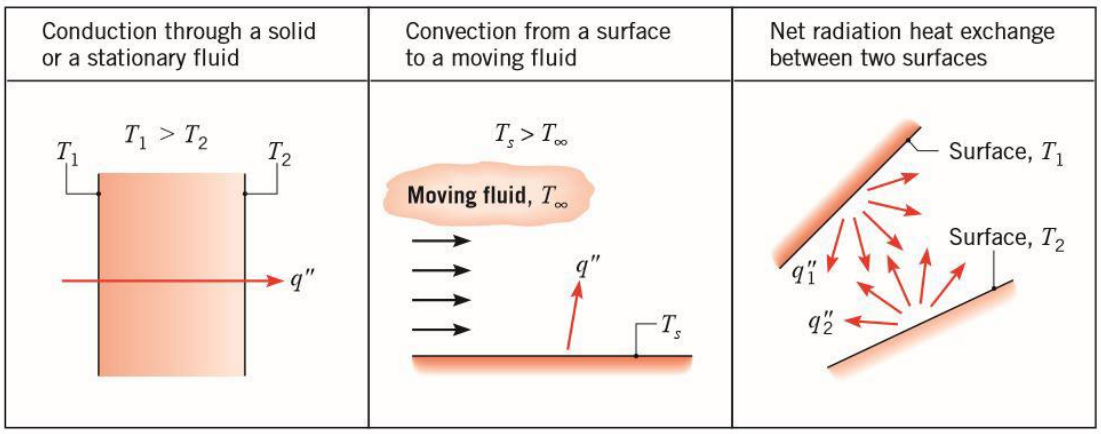

Figure 2.3: A simple demonstration of heat transfer models. q'' is the heat flux, T_s is the surface temperature and T_∞ is the ambient temperature [15].

Firstly, the energy transfer equation is introduced, followed by an explanation of the theory of conduction. Finally, the discussion focusing on the thermal contact resistance, which is a crucial aspect of this project.

2.4.1 Energy transfer equation

The energy transfer through all the possible processes is described by the equation 2.10:

$$\frac{\partial(\rho c_p T)}{\partial t} = -V_j \frac{\partial(\rho c_p T)}{\partial x_j} + k \frac{\partial^2 T}{\partial x_j \partial x_j} + S_T \qquad 2.10$$

where, $\frac{\partial(\rho c_p T)}{\partial t}$ is the accumulation term over time, $-V_j \frac{\partial(\rho c_p T)}{\partial x_j}$ is the convection term, $k \frac{\partial^2 T}{\partial x_j \partial x_j}$ is the conduction term and S_T gives the heat source. The heat source in batteries can be due to the heat generated by Joule effect and the heat generated by the electrochemical reactions. The next part of this section explains the heat transfer methods used in this thesis process and the methodology behind it.

2.4.2 Conduction

When two objects of varying temperatures come in contact, there is a transfer of heat between them, which is known as conduction. This transfer happens due to the random movement of atoms and molecules in the physical mechanism, causing collisions between particles. When particles collide, energy is exchanged, which results in a change in temperature. Conduction is the process of transferring energy within matter. In Figure 5, the left cell is an illustration of conduction through a solid and stationary material.

The heat transfer equation can be written in the 3d form as:

$$q'' = -(k\nabla T) \qquad 2.11$$

Where k is the effective heat transfer coefficient, q'' is the heat flux, and ∇T is the temperature gradient. The negative sign implies the direction of the conduction heat transfer is opposite of the temperature gradient because heat is transferred from a zone of higher temperature to a zone of lower temperature.

2.4.3 Thermal contact resistance

Thermal contact resistance is a parameter used to measure the heat transfer across the interface at the contact of two materials. This parameter is one of the most important parameters in the thermal management systems of Lithium-ion batteries as various types of materials are involved in the thermal management of the batteries. Thermal contact resistance can be defined as follow:

$$R_c = \frac{\Delta T}{q} \qquad 2.12$$

Where ΔT is the temperature drop across the interface of two materials. 'q' is the heat flux through the joint along the perpendicular direction of the contact surface [36].

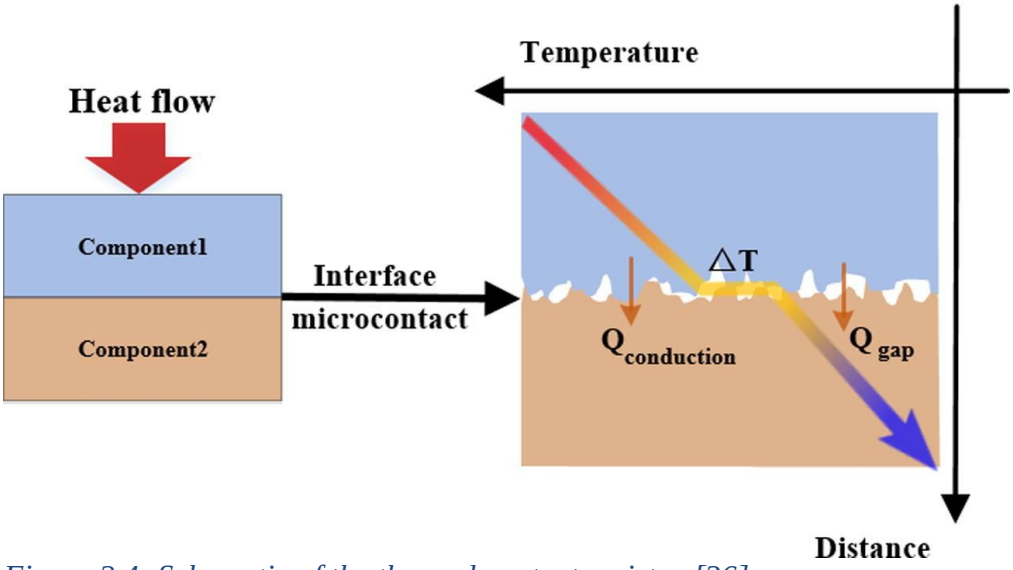

Figure 2.4: Schematic of the thermal contact resistor [36]

Figure 2.4 represents the schematic of the thermal contact resistance. The mechanism of thermal contact resistance is complicated due to several factors affecting it which include factors like the materials across the surfaces, contact pressure, surface roughness, surface waviness, and interface temperature. There are two ways to characterize the thermal contact resistance one being experimental and the other being theoretical.

In experimental terms, the most common way is to place the TIM between the two plates, heat the top plate and cool the bottom plate then [37], calculate the heat flux (Q) that goes through the TIM and measure the temperature drop over the thermal interface material (ΔT). The thermal interface resistance (R_{TIM}) is going to be calculated using the equation [38]:

$$R_{TIM} = \frac{\Delta T}{Q} \qquad 2.13$$

As mentioned in the Section 2.3.1, thermal interface resistance can be written as:

$$R_{TIM} = R_{c_1} + \frac{BLT}{\lambda_{TIM}} + R_{c_2} \qquad 2.14$$

Where R_{TIM} is the total thermal interface resistance, R_{C1} and R_{C2} is the contact resistance at the interface between the TIM and the two surfaces in contact with TIM. λ_{TIM} is the thermal conductivity of the TIM and BLT is the thickness of the TIM. Situations where in the TIM is tested with different thickness and thermal conductivity, the thermal contact resistance can be determined using the linear fit [37] method as shown in Figure 2.5, which is a result of the equation below:

$$R_{TIM} = \frac{BLT}{\lambda_{TIM}} + R_{C1} + R_{C2} = a.(BLT) + b \qquad 2.15$$

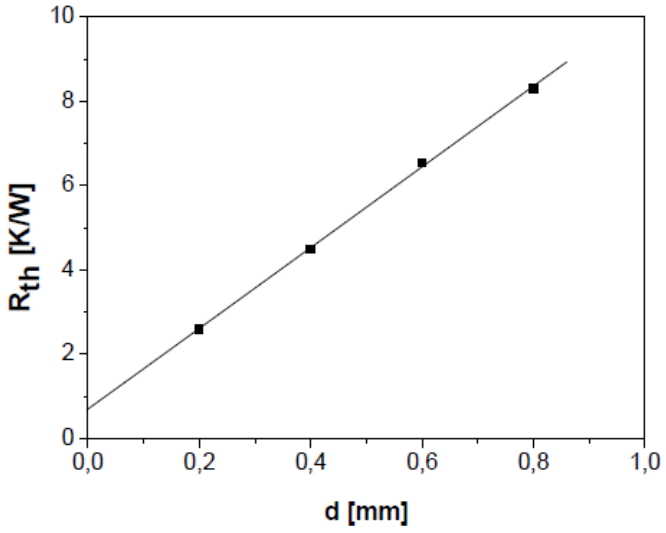

Figure 2.5: The linear fit between thermal interface resistance and the thickness of the TIM [37]

Ralph Schacht [37] determined the thermal conductivity and the thermal contact resistance in the exact same way. Figure 2.6 gives the schematics of his test where he determines the temperature of the silicone (T_{Die}) by the thermal test chip inside the silicone and measures the T_1 and T_2.

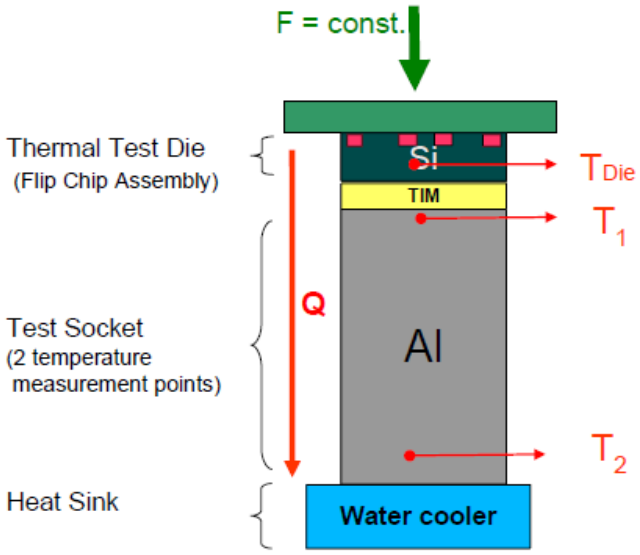

Figure 2.6: Principal schematic for the new test setup [37]

Figure 2.7 shows the schematic of Ralph Schacht's test setup and the equivalent circuit of the TIM.

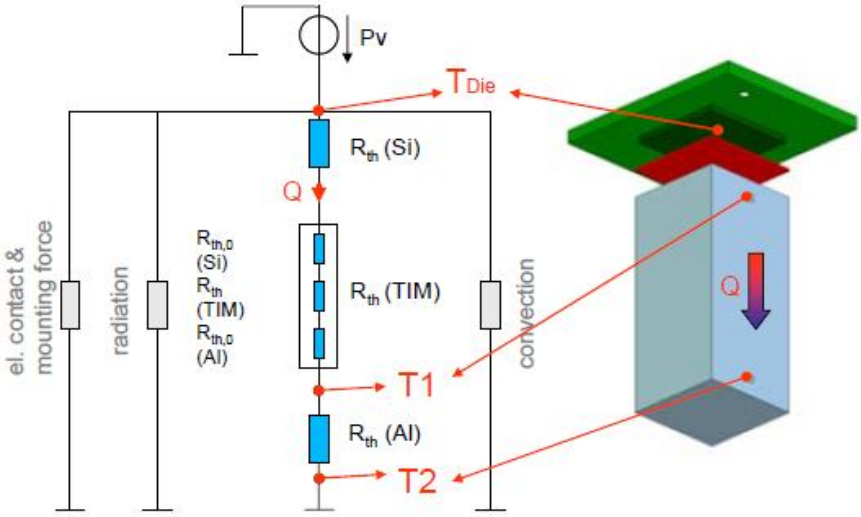

Figure 2.7: Schematic of the thermal equivalent circuit [37]

After measuring T_1 and T_2 and determining T_{Die}, the heat flux is going to be determined by:

$$Q = (T_2 - T_1)\, R_{th_{Al}} \qquad 2.16$$

Where $R_{th_{Al}}$ is the thermal resistance of the aluminum that we already have.
Now the thermal interface resistance of the TIM (R_{TIM}) is going to be determined by the equation:

$$R_{TIM} = \frac{(T_{Die} - T_1)}{Q} - R_{th_{si}} \qquad 2.17$$

where $R_{th_{si}}$ is the thermal resistance of the silicone. He calculates the thermal resistance for different thickness through which he found the thermal conductivity and the thermal contact resistance by the linear fit as explained by Figure 2.8 which demonstrates the result of his study.

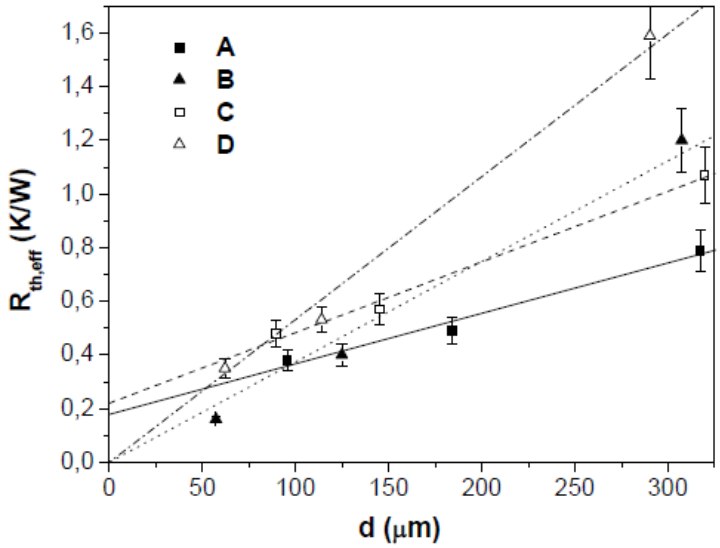

Figure 2.8: Characteristic curve for the different TIM based on the thickness [39]

Figure 2.8 shows that all the points are not exactly in the linear fit line which means that thermal contact resistance is different for different thicknesses. In theoretical sense, thermal contact resistance is complex, and it depends on multiple variables, but mainly, the materials that stick together. Therefore, there is no general theory that can cover all of these variables. However, some theories have proposed to evaluate the thermal contact resistance.

At contact interface the heat is transferred by conduction through the actual contact spots and conduction through the inertial medium such as air. Therefore, the thermal contact conductance is the sum of the thermal conductance through air and through solid.

$$h = h_s + h_g \qquad 2.18$$

where h is the thermal contact conductance, h_s is the thermal conductance through solid and h_g is the thermal conductance through inertial medium like the air [40]. Most of the heat is transferred through solid. To calculate h_s, different theories have been proposed. Most theoretical and experimental studies for solid-solid contact, have related the non-dimensional conductance and the load as [39]:

$$\frac{h_s \sigma}{\acute{\sigma}\, k} = C \left(\frac{F}{H A_a}\right)^n \qquad 2.19$$

Where h_s is the contact conductance σ is the combined standard deviation of the surface heights of the two surfaces:

$$\sigma = \sqrt{\sigma_1^2 + \sigma_2^2} \qquad 2.20$$

σ' is the combined standard deviation of the surface slopes of the two surfaces:

$$\sigma^{'} = \sqrt{\sigma^{'}{}_1^2 + \sigma^{'}{}_2^2} \qquad 2.21$$

k is the harmonic mean of the thermal conductivity:

$$k = \frac{2k_1k_2}{(k_1 + k_2)} \qquad 2.22$$

F is the applied load, A_a is the cross-section area, H is the microhardness of the softer material, C is constant and n is the load exponent. Different studies have shown different values for n and C. The most typical values are $n = 0.95$ and $C = 1.25$ [41].

As it is mentioned in the equation 2.19, one of the most important parameters that affect the thermal contact resistance is the pressure applied to the contact area. M. Williamson [39] designed an experiment to demonstrate the effect of the pressure on the thermal contact resistance. He wanted to see the effect of the surface deformation on the thermal contact resistance as well for which he picked two species, one rough copper and one smooth stainless steel. He then increased the load on the surface gradually and measured the thermal contact resistance. After he reached the highest load, he then decreased the load and again measured the thermal contact resistance. Figure 2.9 demonstrates the measurement of the thermal contact conductance in different pressures for the first loading and unloading cycle and the 10^{th} loading and unloading cycle.

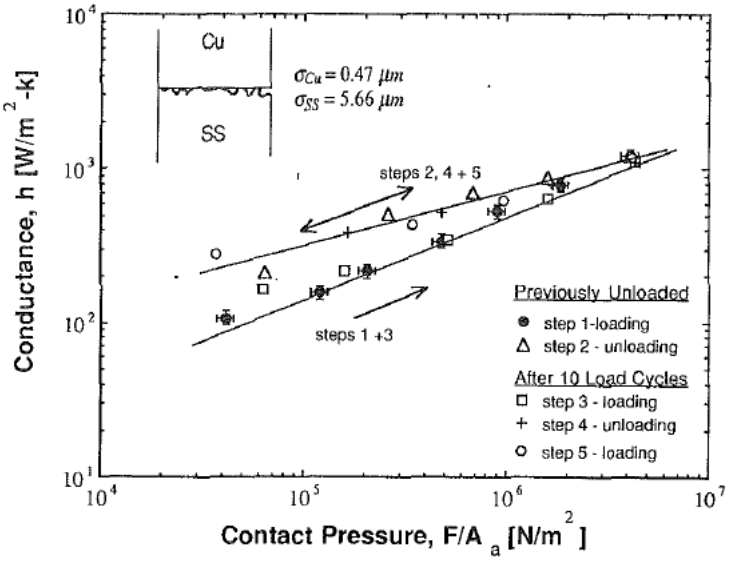

Figure 2.9: Thermal contact conductance between rough stainless steel and smooth copper surface as a function of the contact pressure [39]

Figure 2.9 shows that after ten loading and unloading cycles the thermal contact conductance is higher, which means the deformation of the surfaces helps heat to transfer.

3 Methodology

This section describes the methods and procedures used to conduct this thesis. This project is widely divided into two major aspects: experimentation and simulation. First, the experimental aspect explains in detail the setup, i.e., every component that was used, its characteristics, calibration methods, tolerance limits, sampling rate and data collection methods. Next comes the explanation about how the setup was build, the connections made and how all the components were brought into sync with each other. Post this, the test procedure was explained that gives information about the test conditions and sequence of operations followed, both for the pad and the gel. Later in this chapter, the observations made were highlighted during the experimentation process and finally the limitations about this setup were mentioned.

The simulation part of this section starts with an explanation of the procedure followed in order to simulate a study based on the experimental setup that involved steps like creating a geometry, boundary conditions, mesh study and post-processing of the parameters. This section ends with a detailed explanation of how and what type of relation was established between simulation and experimentation.

3.1 Experimentation

This section explains the equipment used for the experimental setup, building of the setup, the test procedure followed, the data collection and analysis methods, and limitations. Figure 3.1 presents the schematic of the experimental setup.

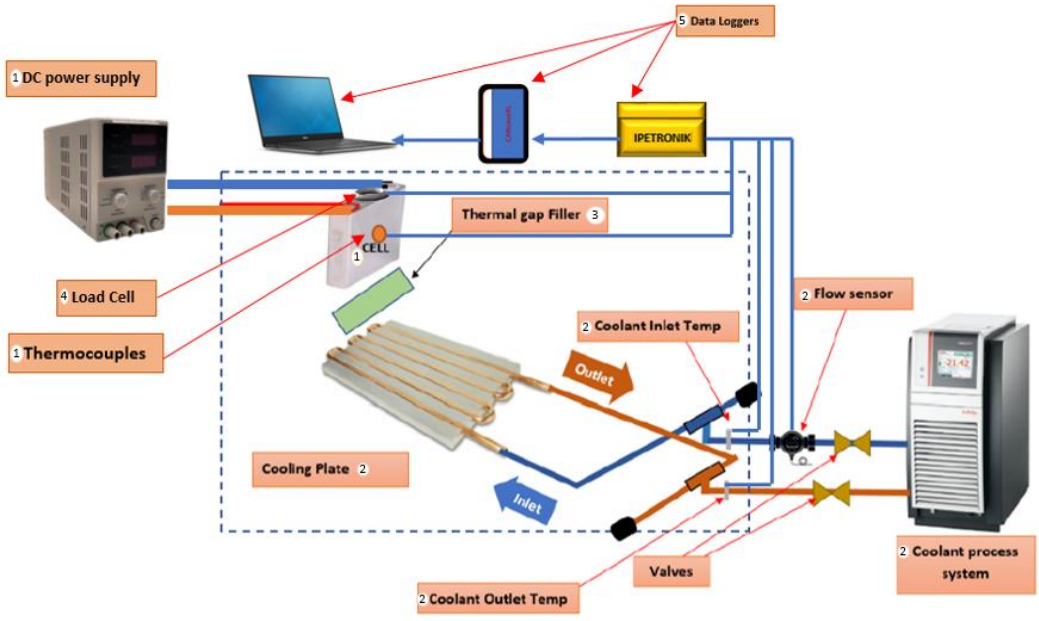

Figure 3.1: Experimental Setup

3.1.1 The experimental setup

This section explains all the parts that were needed for the experimental setup with details and configurations:

- **Dummy cell**

A Toshiba 26Ah stainless steel dummy cell with dimensions as 21 x 114.5 x 104.4 mm as the thickness, length and height was taken into consideration. A 10W heater was placed in the center of the cell which was then covered with Damival U620 grey with hardener H903 Blue resign as a filler material for the heat to be conducted throughout the dummy cell uniformly. The dummy cell was then attached with 5 type-K surface temperature sensors at the top left corner, top right corner, center, bottom left, and bottom right corner respectively with the overall weight of it being 0.48kgs. Figure 3.2 shows the dummy cell on the coolant plate with thermocouples attached.

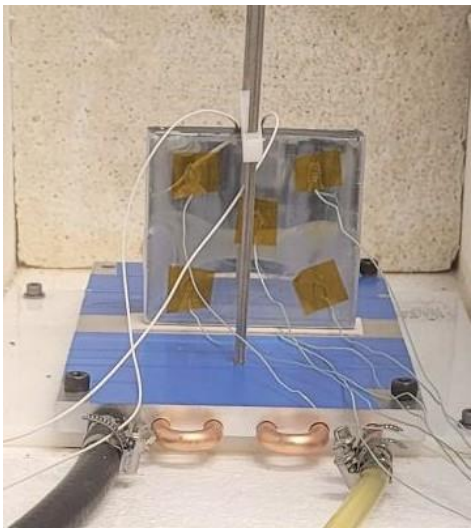

Figure 3.2: Dummy cell with thermocouples and pressure-applying applying mechanism

An RND 320kp KD3000 DC power source with voltage range of 0- 30V and current range of 0 – 5A was used to supply constant current to the heater placed inside the dummy cell for it to heat up and reach a steady state.

- **Cooling system**

A JULABO's air cooled Presto A40 process system with the coolant temperature range of -40℃ to 250℃ and a max pump pressure of 1.7bar at flow rate of 40l/min as shown in Figure 3.3 was used as a cooling system. This system was connected to an ATS-TCP tube cooled cooling plate of dimensions 305 x 15 mm as length and width respectively as shown in the Figure 3.4.

An FT-08 flow sensor from FTI FLOW TECHNOLOGY^{TM} with a range of 0.3 – 30 l/min, calibrated on 20 April 2022, and with an uncertainty of ±0.1% was connected to the inlet of the cooling plate to measure the flow rate of the coolant. In order to make the coolant flow laminar, a laminar flow diffuser was connected before the inlet to the cooling plate. Additionally, inlet and outlet flow PT100 thermocouples were connected to the inlet and outlet pipes respectively to measure the inlet and outlet temperatures of the coolant. These temperatures were important to notice the amount of heat absorbed by the coolant throughout the process.

Figure 3.3: Presto A40 process system

Figure 3.4: ATS-TCP tube cooled plate

- **Thermal interface material (TIM)**

Based on the scope of this project two different TIM materials were tested. TIM 1 is a thermal pad with a thermal conductivity of 3 W/m.K and thickness of 2mm. TIM 2 is a thermal gel with a thermal conductivity of 2.4 W/m.K. TIM 2 was tested with varying thickness of 0.5mm and 2mm. Both the TIMs were put under similar load values of 150N, 300N, 500N and 700N to notice the effect of pressure on thermal resistance properties. Figure 3.5 demonstrates the thermal gel on the cooling plate.

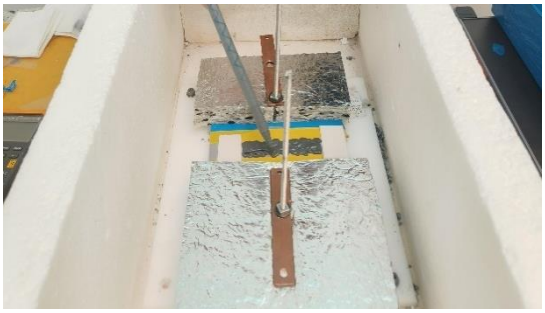

Figure 3.5: Application of Thermal Gel on the coolant plate

The coolant plate was initially wiped off any dust with acetone. In the case of thermal pad, a rectangular portion was cut out from a sheet of the material and pasted on the coolant plate. Rest of the coolant plate was thermally insulated to prevent any heat loss into the atmosphere. After this, the dummy cell was placed on top of the TIM

which was also thermally insulated. A load cell was placed on top of the dummy cell to measure the pressure applied on it.

TIM 2 was applied with different thicknesses on the coolant plate in a similar fashion on top of which the dummy cell was placed. Once the dummy cell was on the TIM 2, it was given 24 hours to be cured at room temperature before the tests could run.

- **Load cell**

An FC23 compression load cell as shown in the figure below, with a range of 50 to 2000lbf was used to measure the load on the dummy cell. It was calibrated using the IPEmotion software before its usage in the test. The dummy cell is shown in Figure 3.6.

Figure 3.6: FC23 compression load cell

- **Data loggers**

The following data loggers from IPETRONIK were used to log the data from the experiment:

- M-THERMO2 – As shown in the Figure 3.7 the M-THERMO2 data logger, previously calibrated on 15 February 2023 with an aggregate sample rate of 800Hz, measurement temperature range of -60℃ to 1370℃ and an uncertainty of ±0.025% was used to log the data from the surface temperature sensors attached to the dummy cell.

Figure 3.7: M-THERMO2

- Mx-SENS24 – The Mx-SENS24 data logger as shown in Figure 3.8, previously calibrated on 20 January 2023 with an aggregate sample rate of 400Hz, measurement current range of 0mA to 20mA and an uncertainty of

±0.30% was used to log the coolant flow rate values from flow sensors attached to the inlet pipe.

Figure 3.8: Mx-SENS24

- M-RTD2 – The M-RTD2 data logger as shown in Figure 3.9, previously calibrated on 23 January 2023 with 400Hz sampling rate, a measurement temperature range of -50℃ to 450℃ and an uncertainty of ±0.020% was used to log the inlet and outlet temperatures of the coolant from the PT-100 thermocouples.

Figure 3.9: M-RTD2

- M-SENS2 – The M-SENS2 data logger as shown in Figure 3.10, previously calibrated on 31 August 2022 with 8Hz sampling rate, a measurement range of 0mA to 20mA and an uncertainty of ±0.05% was used to log the values of pressure applied on the load cell.

Figure 3.10: M-SENS2

- The IPETRONIK data logger is connected to the system through the CANcaseXL as shown in the Figure 3.11.

Figure 3.11: CANcaseXL

- IPEmotion was used to create the DBC file that helped in logging the data from all the data loggers. It was also used to calibrate the load cell. ATI Vision was used as a data acquisition tool that collected signals from the data loggers for a live visual representation of changes in values. MATLAB was used to analyze and manipulate the data for a comparative analysis.

3.1.2 Building the experimental setup

The following sequence of operations had been followed to build the setup:

Dummy Cell:

- A Toshiba dummy cell as shown in Figure 3.2 with the heater inside it was placed on top of the TIM. In case of thermal pad, the tests could be initiated immediately, but for the thermal gel, 24 hours was given for it be cured before initiating the test.
- The heater inside the dummy cell was connected to the RND 320kp KD3000 DC power source with a constant voltage supply of 20V. Based on the math, the current sent to the heater was 8.29Amps.

- 5 surface thermocouples each at the top left, top right, center, bottom left and bottom right were attached on the surface of the dummy cell for its temperature measurement.
- Finally, the dummy cell was insulated on all the surfaces except the bottom surface for the heat transfer to take place vertically downwards, i.e., dummy cell → TIM → coolant plate.
- The FC23 load cell was then placed on top of the dummy cell to which a copper bar was used to apply pressure on top as shown in Figure 3.12.

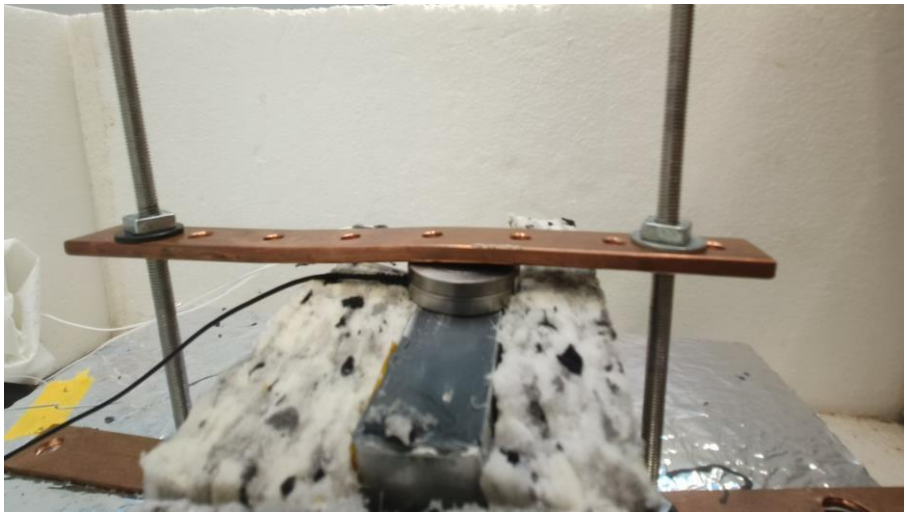

Figure 3.12: Pressure applying mechanism

Cooling System:

- The JULABO's air cooled Presto A40 process system was initially filled with the coolant made of a combination of glycol and water which is then connected to the power supply.
- Next, the coolant input and output connections were made to the ATS-TCP tube cooled coolant plate from the A40 process system to which the PT-100 temperature sensors were connected for sensing the inlet and outlet temperatures of the coolant.
- In addition, an FT-08 Flow sensor was attached right before the input to the coolant plate to measure the flow of the coolant flowing into the plate, the other end of which is connected to a laminar flow diffuser to make the coolant flow laminar for a better certainty of heat absorption.
- The coolant plate was thermally insulated with Styrofoam and then screwed inside a Styrofoam box for thermal insulation of the entire setup.

Thermal Interface Material:

- First, the thermal pad of 2mm thickness was cut out into 25 x 120 mm, which is larger and wider than the bottom surface area of the dummy cell.
- The TIM was then placed at the center of the cooling plate across the coolant pipes.
- Apart from the area occupied by the TIM, the rest of the coolant plate was thermally insulated with Styrofoam to prevent heat loss.
- To introduce a new TIM, the old TIM could be simply replaced with the new one and its thickness could be set accordingly.

Data loggers:

- The surface thermocouples were connected to the M-THERMO2 data logger.
- The PT-100 temperature sensors were connected to the M-RTD2 data logger.
- The FT-08 flow sensors were connected to the Mx-SENS24 data logger.
- The loadcell was connected to the M-SENS2 data logger.
- The above-mentioned data loggers were connected to the laptop through the Vector CANcaseXL.

Software:

- After all the connections were made, the database (dbc) file needed to calibrate the load cell and input the parameters for data logging was created using the IPEmotion software.
- Finally, this dbc file was inputted into the ATIVision software that was used to for visual representation of the data.
- MATLAB was then used to manipulate and plot the results.

3.1.3 Procedure

The agenda to perform this experiment was to investigate the changes in the thermal resistive properties of two different kinds of TIMs by altering their parameters in a steady-state situation. The parameters being the thickness of the TIM and pressure applied on the TIM.

- **Test Conditions**

The following test conditions were used:

Table 3.1: Test conditions for thermal pad

S.No	Parameter	Value	Unit
1	TIM	Thermal Pad	-
2	Thickness of TIM	2	mm
3	Thermal Conductivity	3	W/m.K
4	Forces applied	4.8,150,300,500,700	N
5	Coolant temperature	20	℃
6	Coolant pressure	1	bar
7	Time taken for coolant to stabilize	45	minutes
8	Time for the entire test	270	minutes
9	Power supplied to dummy cell	10	Watts

From the Table 3.1 it can be noticed that for the thermal pad all the parameters were kept constant, but the force applied was altered. For the first test, it was only the weight of the dummy cell that was acting on the TIM. Later, the force was incremented gradually with a difference of approximately 200N to notice the changes in thermal resistive properties of the TIM.

Table 3.2: Test conditions for thermal gel

S.No	Parameter	Value	Unit
1	TIM	Thermal Gel	-
2	Thickness of TIM	2,0.5	mm
3	Thermal Conductivity	2.4	W/m.K
4	Forces applied	4.8,150,300,505,685	N
5	Coolant temperature	20	℃
6	Coolant pressure	1	bar
7	Time taken for coolant to stabilize	45	minutes
8	Time for the entire test	270	minutes
9	Power supplied to dummy cell	10	Watts

From the Table 3.2 it can be noticed that for every thickness of the thermal gel, the pressure applied was incremented with a difference of approximately 200N, initial test with only the weight of the dummy cell, to notice the changes in thermal resistive properties of the TIM.

- **Test Procedure**

The following sequence of operations were performed for both TIM1 and TIM2:

- Apply a specific amount of force to the dummy cell and wait until the load cell data stabilizes.
- Start recording.
- Adjust the coolant temperature to 20℃, regulate the pressure to 1 bar, and activate the coolant flow.
- Allow 45 minutes for the coolant flow to stabilize and the setup to reach 20℃.
- Set the DC power supply to the CV mode and supply a constant voltage of 12V to the heater inside the dummy cell.
- After 270 minutes, end the test and collect the test data.

3.1.4 Experiment limitations

This timeline for this project was limited to the spring of 2023 with limited access to the components used in the realistic word. Due to this, several assumptions and limitations were implemented to get the best possible output. One of the first limitation was to use a dummy cell and not a real cell. There are multiple reasons for this consideration, first being, our project was based on the heat transfer aspects of the TIM but not on the source of heat, due to which the electrochemistry part of the real cell was neglected. Secondly, we wanted to perform a comparative analysis under steady-state conditions, for which the heat generated in the battery was simplified as a constant heat flux, instead of space, time and drive-cycle dependent. Along with that, the mechanical properties of the cell, which include, dimensional stability, mechanical strength, elasticity, fatigue resistance, thermal expansion were also not taken under consideration. To avoid the heat loss from the dummy cell to the surrounding environment, the cell was thermally insulated with foam material from all the sides except the bottom surface through which heat was supposed to pass to the TIM and thereby to the cooling plate.

In the case of thermal gel, it was not an easy task to maintain a specific thickness as it was a semi-solid material made of two components. Due to this, a solid material of respective thickness was placed on either corners of the coolant plate and then the gel was applied. In the end, the dummy cell was placed on top of the gel with little pressure applied to avoid the air gaps. Later it was given 24 hours to be cured post which tests were run. Another important limitation was that two different dummy cells were used through the process of this experimentation, one for the thermal pad and other for the thermal gel. Due to this there was a difference in the heat gradient on the surface of the dummy cell as both were not built exactly like each other. It is also important to note that the heater inside the dummy cell was not placed exactly at the center, as shown in the Figure 3.15, due to which the temperature distribution is irregular on the surface of the cell.

Throughout the tests, the incoming coolant properties and dummy cell conditions were kept constant to enable a comparative study between different TIMs and same TIM of varying thicknesses. Thermal insulation using Styrofoam was done on the coolant plate as well, except the part where the TIM is placed to avoid heat loss into the surroundings. The mechanism used to apply pressure on the TIM was done by applying a point load on the load cell that was placed on top of the dummy cell rather than applying force on the entire area. This was done to the best of our knowledge due to the lack of access to ideal components. Nevertheless, since this was a comparative study, it was possible to investigate and suggest improvements of the heat transfer. Lastly, the entire setup was insulated from the environment to avoid convective heat losses into the surrounding atmosphere.

3.2 Simulation

To gain a better understanding of the experiment and determine the equivalent thermal resistance of the TIM, a thermal simulation was conducted that replicated the experimental tests. The simulation was performed using Star CCM+ software, the sequence of operations of which is illustrated in Figure 3.13.

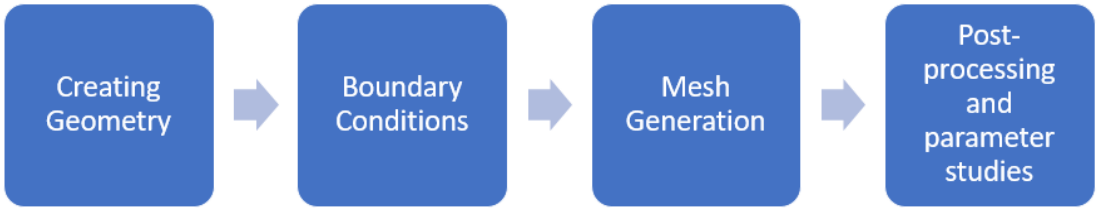

Figure 3.13: Steps of the simulation methodology

3.2.1 Procedure

At the beginning of this chapter, an overview is provided of the simulation process, followed by a detailed explanation of each step. Initially, the geometry of the equipment used in the experiment was created. Then, the thermal properties and boundary conditions were assigned to the parts. Next, a mesh was generated to represent the simulation model and finally, the results were post-processed and presented.

- **Creating geometry**

The dimensions of a real Toshiba 26Ah cell were used to create a geometry for a dummy cell. The dummy cell consists of the dummy cell, a heater inside the dummy cell, the material filling the dummy cell, and the TIM. The Table 3.3 provides the characteristics of each of these subparts.

Table 3.3: Specifications of dummy cell components

Part name	Thermal conductivity	Comments
Dummy Cell	15.1	Stainless steel dimensions: 21 * 114.5 * 104.5 mm Thickness: 0.5 mm.
The material filled in the dummy cell	2.4	Thermal gel from Von Roll company used to fill the space between the dummy cell and the heater
Heater	398	Copper dimensions: 100 * 100 mm Thickness: 1.4mm
TIM 1(Thermal pad)	3	Thickness: 2mm
TIM 2(Thermal gel)	2.4	Thickness: 3mm, 2mm, 0.5 mm

The geometry of the simulation is shown in Figure 3.14 which the grey box is the dummy cell, the green part is the material inside the dummy cell and the blue part is the TIM.

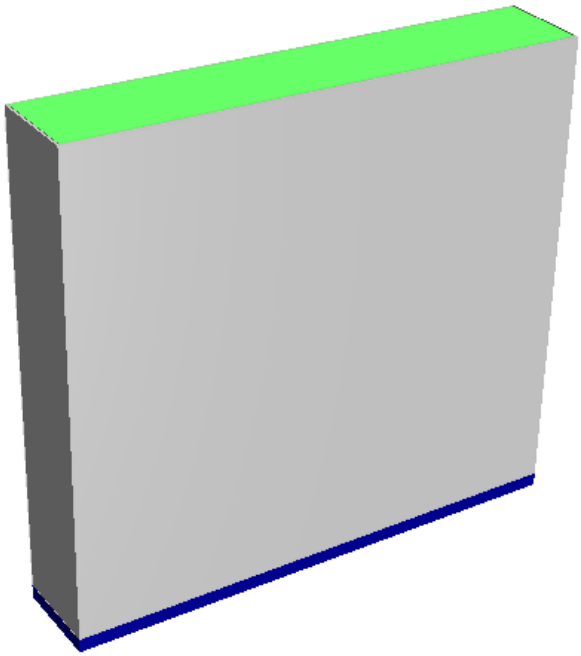

Figure 3.14: Geometry of the simulation

Figure 3.15 gives the cross-section view of the geometry which shows the positioning of the heater inside the dummy cell. The red rectangle is the heater, located at the

center of the dummy cell, green part being the material the dummy cell was filled with and the grey boundary being the dummy cell.

Figure 3.15: Cross section of the geometry of the simulation

- **Boundary conditions**

In the simulation, the goal was to replicate the exact conditions present in the experimental setup. The cell's boundary was made adiabatic since it was insulated. The bottom of the thermal interface material was assumed to have a constant temperature. This was because the coolant flow rate running through the cooling plate was sufficiently high to consider the cooling plate temperature constant. The boundary conditions used in the simulation are shown in Figure 3.16.

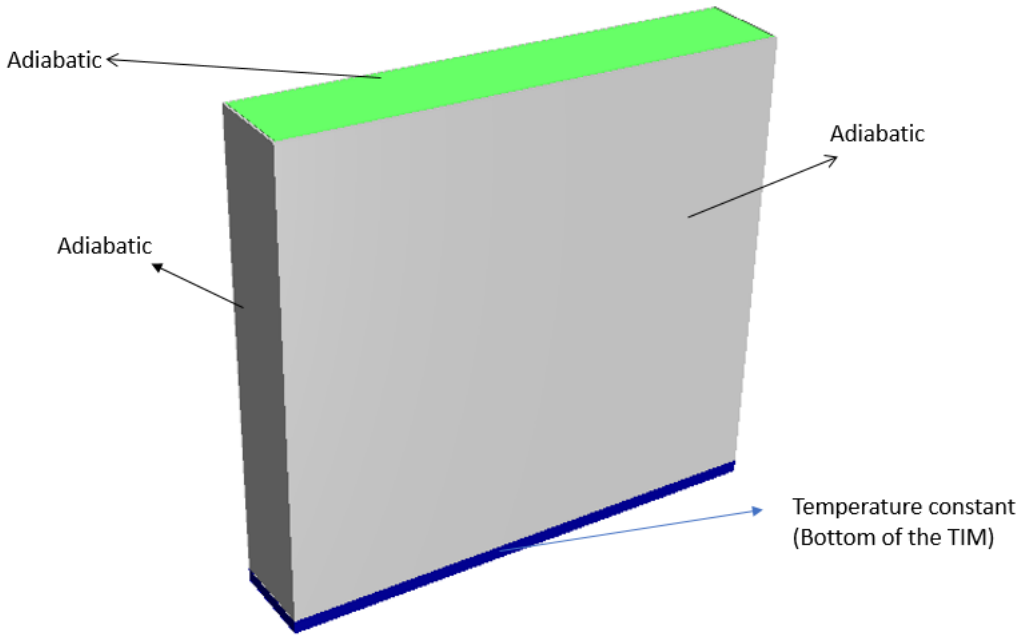

Figure 3.16: Boundary conditions of the cell

- **Mesh generation**

The mesh was generated using Star CCM+ Auto mesh. To achieve better accuracy of heat conduction in the thin layers of the dummy cell and the thermal interface material, seven mesh layers were used. A mesh study was conducted to ensure that the results were independent of the mesh. Figure 3.17 demonstrates the thin layer mesh for TIM and Figure 3.18 presents the thin layer mesh for the dummy cell.

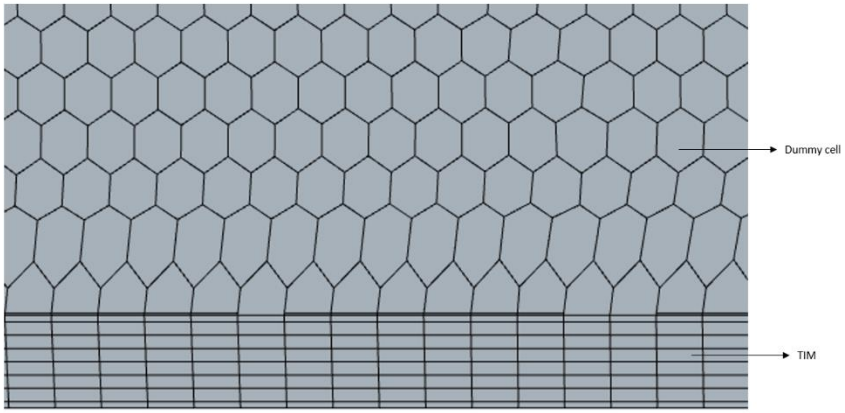

Figure 3.17: Close look at the mesh of the TIM

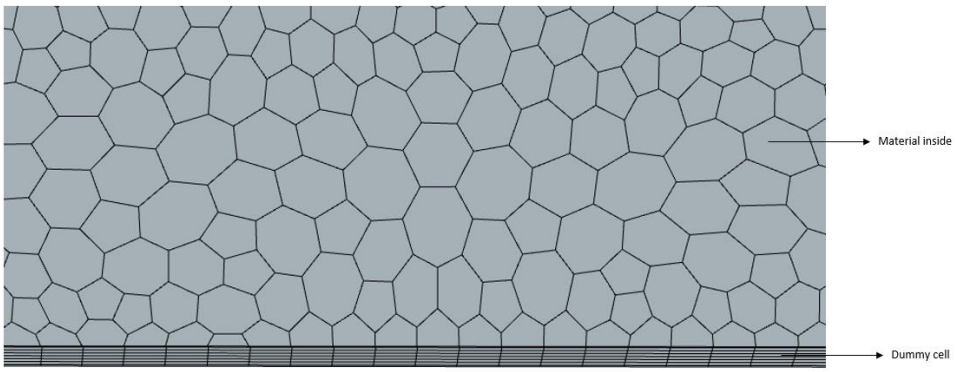

Figure 3.18: Close look at the mesh of the dummy cell

To conduct the mesh study, three different cases were run, each with a different maximum cell size. In all the cases, the thin layer mesh with seven layers was used to ensure the accuracy of heat transfer in the thin layers. Since the maximum cell size was different in these three meshes, the number of cells varied as well. The temperature at the center and the heat transfer at the bottom of the TIM were compared across different mesh refinements as shown in the table below:

Table 3.4: Cell number of the components inside the dummy cell

	Max cell size [mm]	Cells no. of the heater	Cells no. of the dummy cell	Cells no. of the material inside the dummy cell	Cells no. of the TIM	Total cell no.
Refinement 1	15	42811	119393	56952	11008	230164
Refinement 2	10	88223	262029	120701	25946	496899
Refinement 3	9	101706	321086	155453	32219	610464
Refinement 4	8	138204	473399	217348	35007	863958

Table 3.5: Characteristics of each of the refinements

	Heat transfer (w)	Deviation	Center temp (C)	Deviation
Refinement 1	9.999821	1.79e-4	35.39	0.07
Refinement 2	9.999995	5e-6	35.35	0.03
Refinement 3	10.00000	0	35.32	0
Refinement 4	10.00000	-	35.32	-

As demonstrated, in refinement 3, the error was zero, indicating that the simulation was independent of the mesh. Therefore, refinement 3 was used for all subsequent simulations as shown in the Figure 3.19.

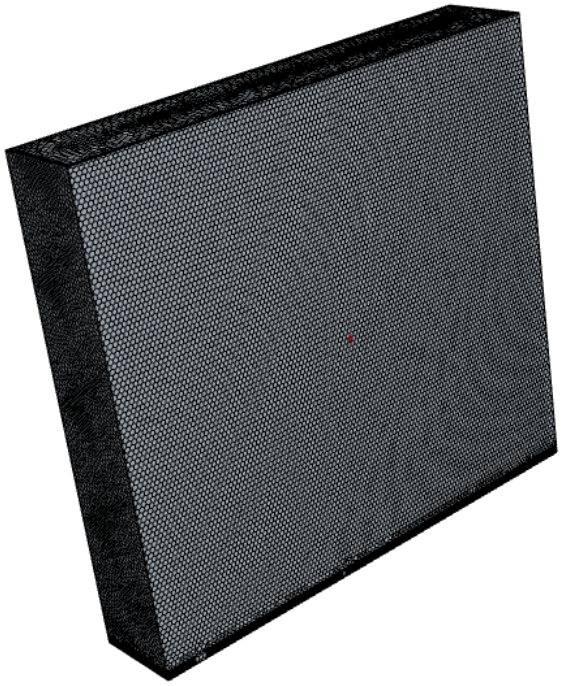

Figure 3.19: 3D view of the mesh

- **Post-processing and parameter study**

The thermal resistivity of the TIM can be characterized by the thermal interface resistance shown in the equation below:

$$R_{TIM} = R_{C1} + \frac{BLT}{\lambda} + R_{C2} \qquad 3.1$$

Thermal interface resistance includes the thickness of the TIM, the thermal contact resistance, and the thermal conductivity of the TIM. When TIM is under pressure, thermal interface resistance can be changed because of the change in the thermal contact resistance (R_{C1} and R_{C2}) and the thickness. The alternate equation for thermal interface resistance can be written as:

$$R_{TIM} = \frac{BLT_{base}}{\lambda_{eff}} \qquad 3.2$$

where BLT_{base} is the base thickness of the TIM and the λ_{eff} is the effective thermal conductance.

3.3 Experimentation and simulation: a complimentary approach

In this study, a TIM with a specific base thickness was applied between a dummy cell and a heat sink, and the temperature profile of the dummy cell was determined experimentally under different pressure conditions. A numerical simulation was conducted in parallel to the experimentation to determine the temperature profile of the dummy cell at different thermal interface resistances of the TIM. These temperature profiles of each experimental case were compared to that of the simulation, with the help of which the thermal effective conductance and thermal interface resistance of the TIM were determined. Using this data, the necessary plots were plotted as discussed in the Results & Discussions.

It is important to note that there were limitations that prevent a perfect simulation of the experiment. For instance, the walls of the dummy cell were insulated and adiabatic, but there is always some heat loss. Therefore, the effective thermal conductance and thermal interface resistance may have some error. However, since this is a comparison study and all cases were experimented under the same conditions, the error for all cases is nearly the same. By comparing the different thermal interface resistances, it is possible to determine the optimized conditions for applying the TIM between the heat sink and the battery.

4 Results & Discussions

This chapter is divided to 3 sections: simulation, experimentation, and comparative analysis. In the simulation section, the temperature profile of the dummy cell with 2mm TIM and a thermal conductivity of 3 W/m.K is presented. Next, a parameter study has been conducted to obtain the relation between the thermal interface resistance of the TIM and the center temperature of the dummy cell.

In the experimentation section, the surface temperature profile of the dummy cell with 2mm thermal pad of 3W/m.K is presented and compared with the temperature profile of the dummy cell in the simulation section. In the comparative analysis section, the steady-state temperature of the cell under different pressures is compared. Next, with the help of the parameter study, the thermal interface resistance of the different pressure cases is compared and finally a relative thermal interface resistance vs pressure plot is generated to better understand the change in thermal resistive properties of the TIMs with pressure applied.

4.1 Simulation

Figure 4.1 presents the temperature profile of the dummy cell with a 2mm TIM with a conductivity of 3 W/m.K. It can be seen that the highest temperature at the top of the cell is 37.6℃ and at the bottom is 20℃ which matches that of the dummy cell in the experimentation phase.

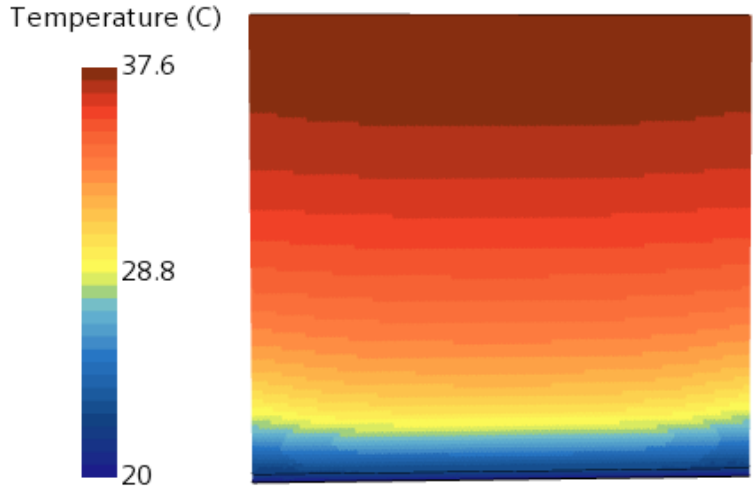

Figure 4.1: Temperature profile of the simulation

Figure 4.2 demonstrates the behavior of the cell temperature with the change in effective thermal conductivity of the TIM. This is shown for all different thicknesses of the TIM. The trend shows that increasing the thermal effective conductivity of the TIM the center temperature of the cell decreases.

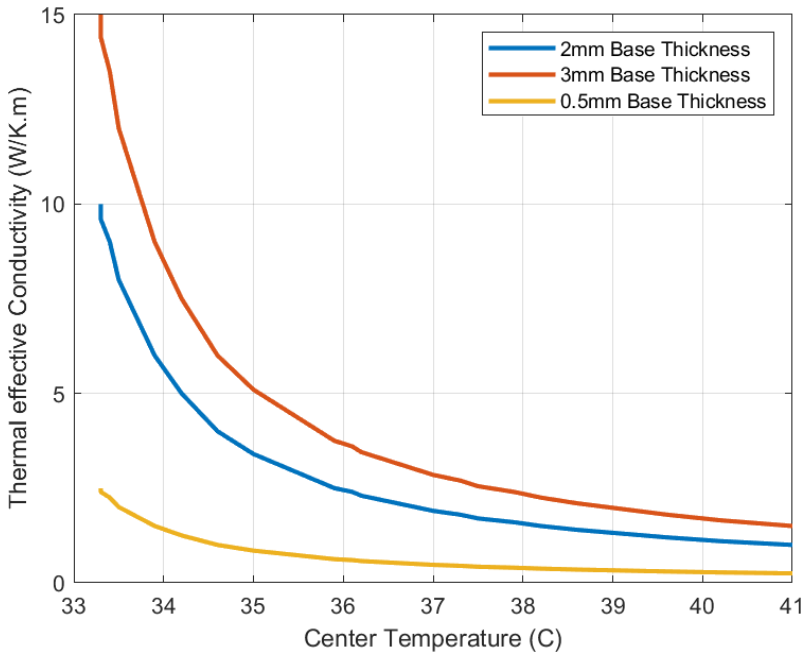

Figure 4.2: Cell center temperature vs thermal effective conductivity for different thicknesses

Figure 4.3 presents the behavior of the cell temperature when the thermal interface resistance of the TIM is changing.

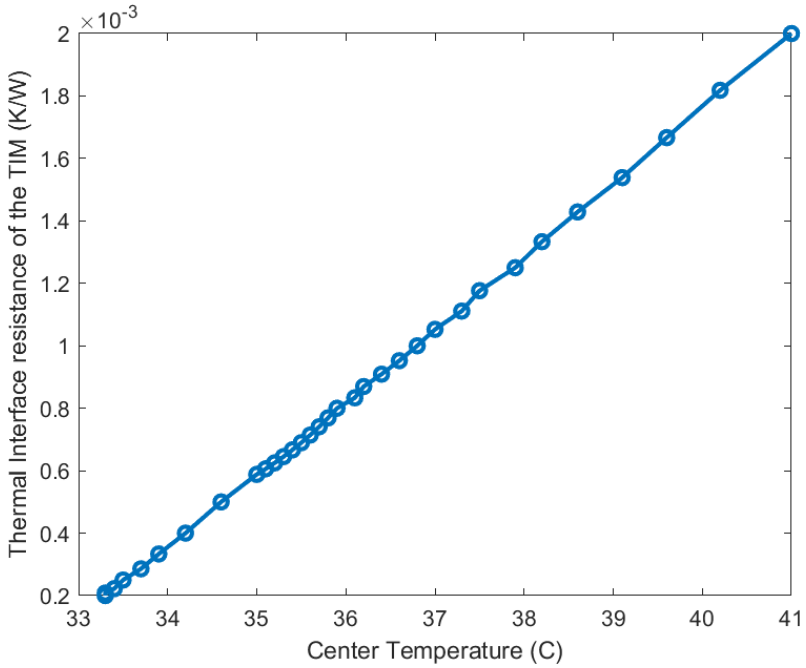

Figure 4.3: Thermal interface resistance vs the cell center temperature for the TIM

As it is presented the temperature of the cell is increasing linearly with increase in the thermal interface resistance.

4.2 Experimentation

4.2.1 Temperature behaviour of dummy cell

The Figure 4.4 shows the temperature behavior of the dummy cell with the usage of 2mm thermal pad under no pressure applied with the test conditions as mentioned in the section 3.1.3.

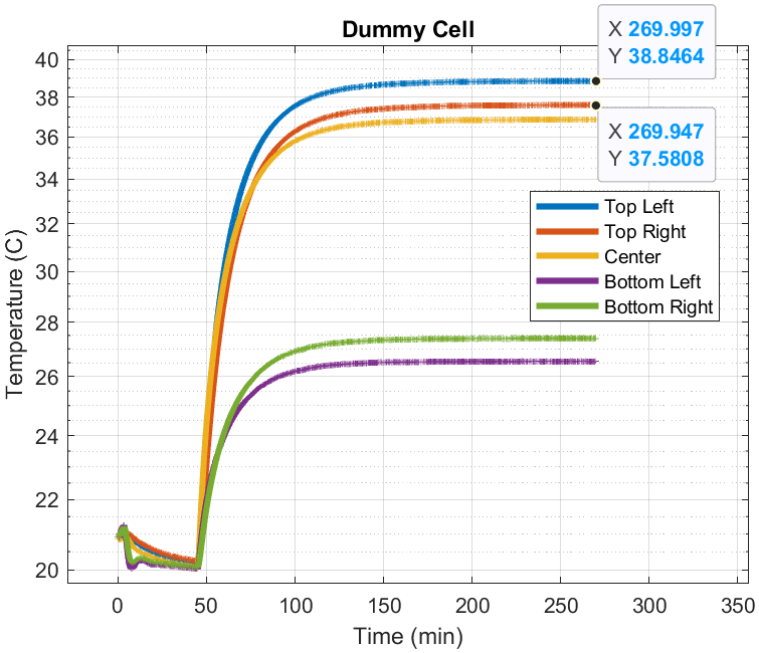

Figure 4.4: Temperature profile of the dummy cell with thermal pad under no pressure conditions

It can be noted that initially when the recording started, the setup was given 45 minutes for the coolant to be stabilized and the setup temperature to reach the room temperature conditions. Post the stabilization, the power supply to the heater was switched on and the test was run for a total of 270 minutes for the dummy cell to reach steady state conditions after which data was extracted.

It is worth mentioning from the Figure 4.4 that the temperature of the dummy cell at top left is Y=38.84℃ and top right is Y=37.75℃ by the end of the test which is not the same. This is unlike the simulation in which the horizontal temperature profile remains constant as shown in Figure 4.1. The reason for this is the inability for the heater to be placed exactly at the center of the dummy cell as explained in section 3.1.4.

4.3 Comparative analysis – thermal pad and thermal gel

In this section, the steady state temperature at different pressures is compared for the thermal pad of 2mm thickness, thermal gel of 2mm thickness and thermal gel of 0.5 mm thickness. After that with the help of the parameter study of the simulation, the thermal interface resistance of the TIM at different pressure is compared.

4.3.1 Thermal Pad

The Figure 4.5 gives the relationship between the steady-state temperature of the dummy cell and the pressure applied on the thermal interface material.

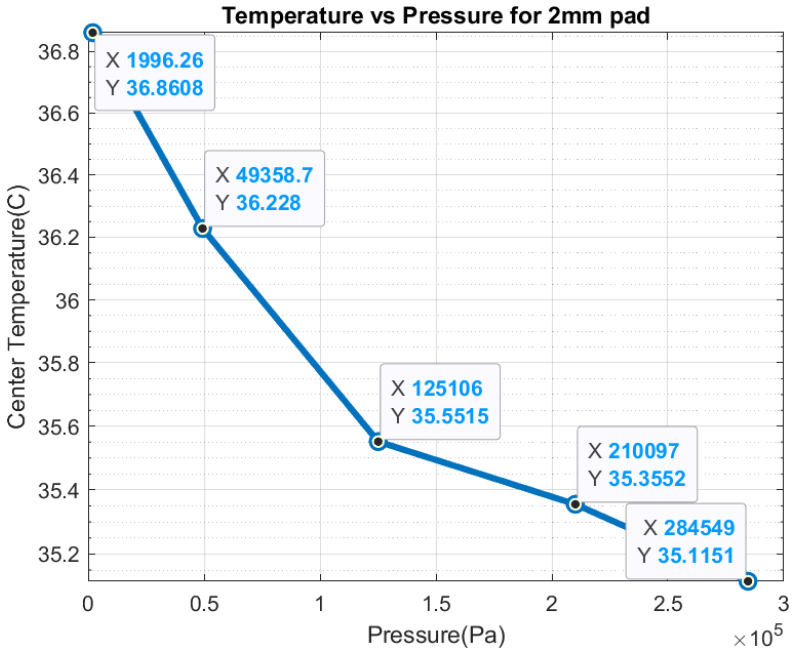

X-Center Temperature (℃)
Y- Pressure (Pa)
1 bar = 1 x 10^5 Pa

Figure 4.5: Center temperature vs pressure applied to the TIM for the thermal pad

The experimental findings demonstrate that an increase in pressure applied to the Thermal Interface Material (TIM) leads to a decrease in the center temperature of the dummy cell, indicating an improvement in pad performance. Initially, the temperature of the cell was recorded as Y=36.86 ℃. Subsequently, as pressure was introduced at X=0.49 bar, the temperature decreased to Y=36.22℃. Further increasing the pressure to X=1.2 bar resulted in a temperature drop to Y=35.55℃. The temperature continued to decrease as the pressure was raised to X=2.1 bar, reaching 35.35℃, and finally, at X=2.8 bar, the temperature reached Y=35.15℃. Overall, employing a 2mm thermal pad with a conductivity of 3W/m.K led to an approximate 5% reduction in the dummy cell's temperature.

Considering Figure 4.5, Figure 4.3 and the complementary study between simulation and experimentation, Figure 4.6 was generated which gives the relation between the thermal interface resistance of the TIM vs the pressure on it. Initially, the thermal interface resistance is at Y=10 x 10^{-4} K/W. Subsequently, it decreases to Y=8.6 x 10^{-4} K/W when pressure reaches X=0.49bar. As pressure increases to X=1.2bar, the interface resistance comes down to Y=6.8 x 10^{-4} K/W. Later at pressure X=2.1bar, Y=6.4 x 10^{-4} K/W and finally, at pressure X=2.8bar, the thermal interface resistance reached a value of Y=6 x 10^{-4} K/W.

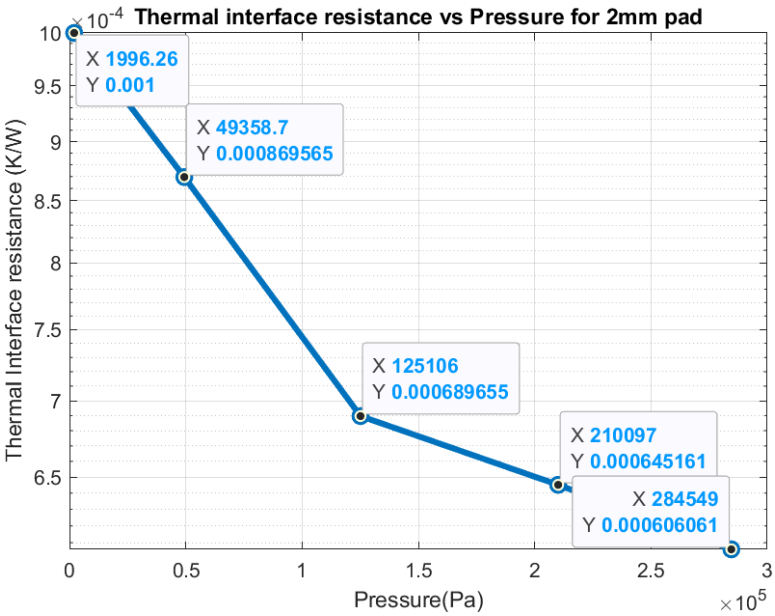

X-Thermal Interface Resistance (K/W)
Y- Pressure (Pa)
1 bar = 1 x 10^5 Pa

Figure 4.6: Thermal interface resistance vs Pressure for thermal pad

Figure 4.7 gives a better representation of the change in thermal interface resistance vs pressure. If the thermal interface resistance at no pressure condition is considered to be 100%, then the figure shows that there is approximately a 40% reduction in the thermal interface resistance of the thermal pad at the highest-pressure X=2.8bar.

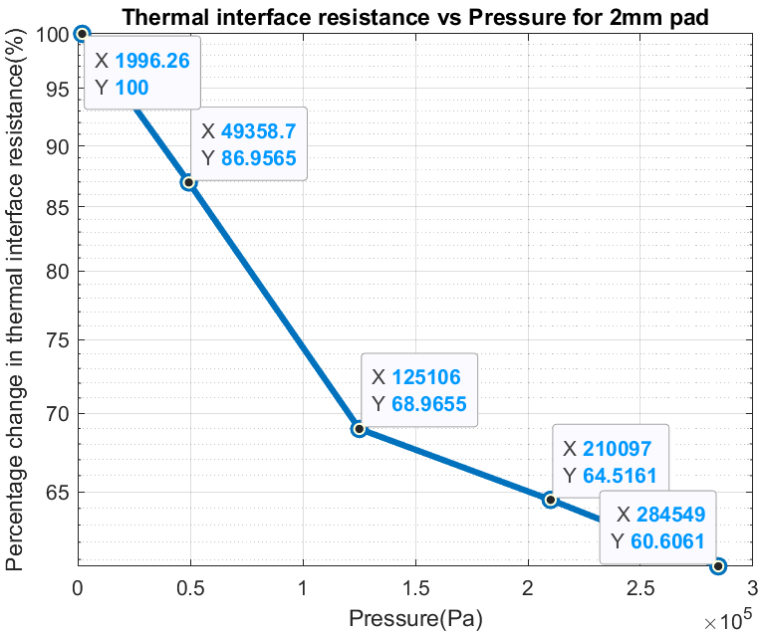

X- % change in Thermal Interface Resistance
Y- Pressure (Pa)
1 bar = 1 x 10^5 Pa

Figure 4.7: Percentage change in thermal interface resistance for thermal pad

4.3.2 Thermal Gel

As explained in section 3.1.3, 2mm and 0.5mm thicknesses of thermal gel were experimented with different pressures applied to them and the results are presented below:

2mm thermal gel

Figure 4.8 presents how steady state temperature changes by changing the pressure for 2mm thermal gel TIM.

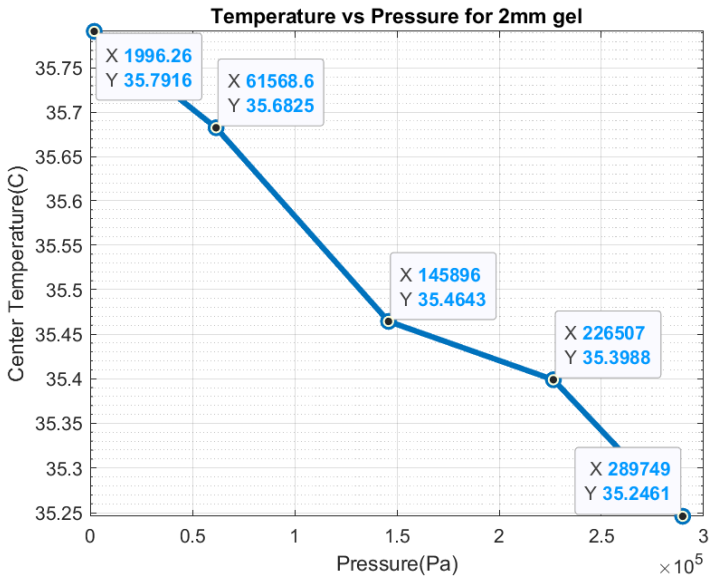

X-Center Temperature (℃)
Y- Pressure (Pa)
1 bar = 1 x 10^5 Pa

Figure 4.8: Temperature of dummy cell vs pressure applied on 2mm gel

Observing the data, it is evident that the application of pressure leads to a decrease in the center temperature. Initially, the temperature is recorded as Y=35.79℃. As pressure is applied, the temperature decreases to Y=35.68℃ at X=0.61bar. With an increase in pressure to X=1.4bar, the temperature further decreases to X=35.46℃. Continuing to increase the pressure to X=2.2bar, the temperature drops to Y=35.39℃, and finally, at X=2.8bar, the temperature reaches Y=35.24℃. Overall, there is an approximate 1.5% reduction in the cell temperature when using a 2mm thermal gel.

Using the complimentary study, the Figure 4.9 was generated which showcases the relationship between thermal interface resistance and pressure applied.

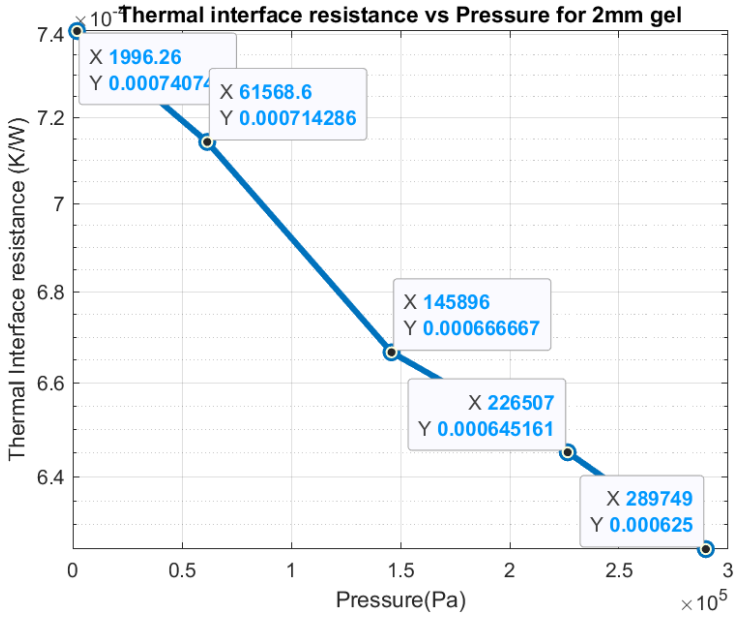

X-Thermal Interface Resistance (K/W)
Y- Pressure (Pa)
1 bar = 1 x 10^5 Pa

Figure 4.9: Thermal interface resistance vs Pressure for 2mm thermal gel

Initially the thermal interface resistance is at Y=7.4 x 10^{-4} K/W. Next, it comes down to Y=7.1 x 10^{-4} K/W at pressure X=0.61bar. Upon increasing the pressure to X=1.4bar, resistance came down to Y= 6.6 x 10^{-4} K/W. Later at pressure X=2.2bar the resistance had a value of 6.4 x 10^{-4} K/W and finally at pressure X=2.8bar, the value of Y reached to 6.2 x 10^{-4} K/W.

Figure 4.10 gives a better representation of change in thermal interface resistance vs pressure. If the thermal interface resistance at no pressure condition is considered to be at 100%, then the figure shows that there is approximately a 15% reduction in the thermal interface resistance of the 2mm thermal gel at the highest-pressure of X=2.8bar.

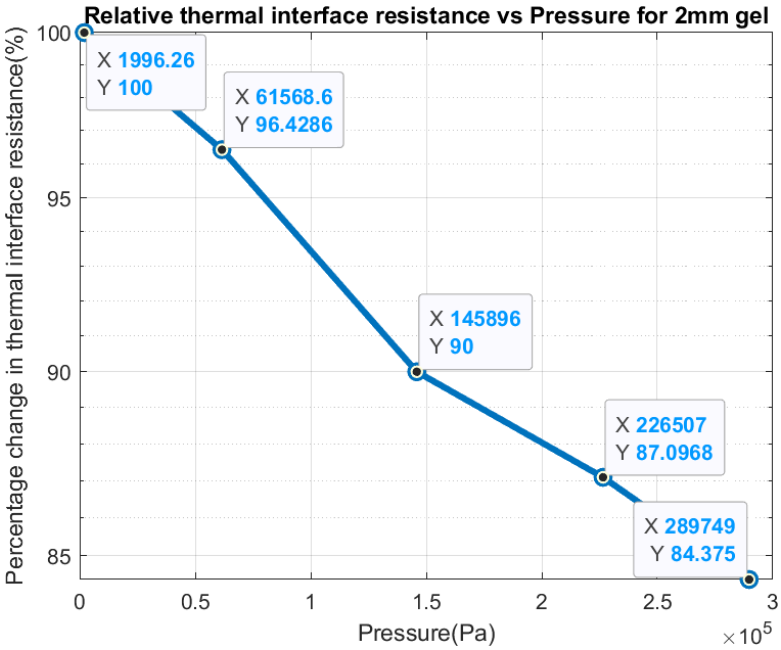

X- % change in Thermal Interface Resistance
Y- Pressure (Pa)
1 bar = 1 x 10^5 Pa

Figure 4.10: Percentage change in thermal interface resistance for 2mm thermal gel

0.5mm thermal gel

Figure 4.11 presents how steady state temperature change by changing the pressure for 0.5mm thermal gel TIM. Initially the temperature of the cell was recorded as Y=34.85℃. Subsequently, as pressure increased to X=0.61bar, the temperature decreased to Y=34℃. Further increasing the pressure to X=1.4bar, the temperature came down to Y=33.89℃. Contrary to the trend, increasing the pressure to X=2.2bar and further to X=2.8bar, the temperature of the cell increased to Y=33.91℃ and later to Y=34.15℃.

Upon investigation, it was found out that the surface of the thermal glue of 0.5mm thickness developed cracks at pressure X=1.4bar and encountered damage. This damage resulted in air gaps formation due to which the performance of the gel worsened as the experiment progressed.

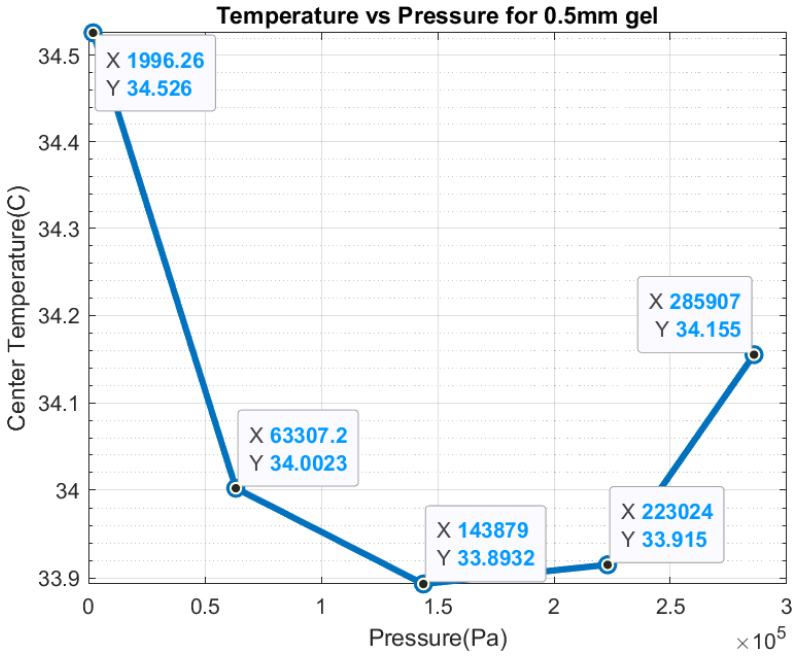

X-Center Temperature (°C)
Y- Pressure (Pa)
1 bar = 1 x 10^5 Pa

Figure 4.11: Temperature of dummy cell vs pressure applied on 0.5mm gel

Figure 4.12 presents the thermal interface resistance vs the pressure applied on the TIM for thermal gel 0.5 mm. Initially the thermal interface resistance is at X=4 x 10^{-4} K/W under no pressure condition. Next it comes down to Y=3.5 x 10^{-4} K/W at pressure Y=0.6bar. As pressure is increased to X=1.4bar the resistance came down to 3 x 10^{-4} K/W. Now, due to the damage on the surface of the gel, the resistance increased to Y=3.3 x 10^{-4} K/W at pressure X=2.2 bar and further increased to Y=3.8 x 10^{-4} K/W at X=2.8bar.

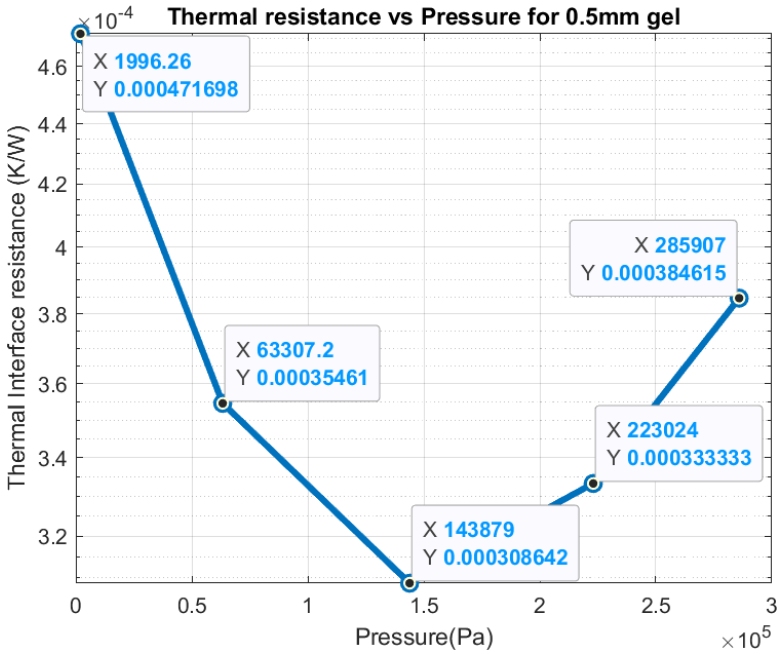

X-Thermal Interface Resistance (K/W)
Y- Pressure (Pa)
1 bar = 1 x 10^5 Pa

Figure 4.12: Thermal resistance vs Pressure applied on 0.5mm gel

Figure 4.13 gives a better representation of change in thermal interface resistance with pressure increase. If the thermal interface resistance under no pressure situation is considered to be 100%, it reduced by approximately 35% at pressure X=1.4bar and

due to the damage on the surface of the gel and presence of air gaps, the resistance increased by 16% by the time pressure was at X=2.8bar.

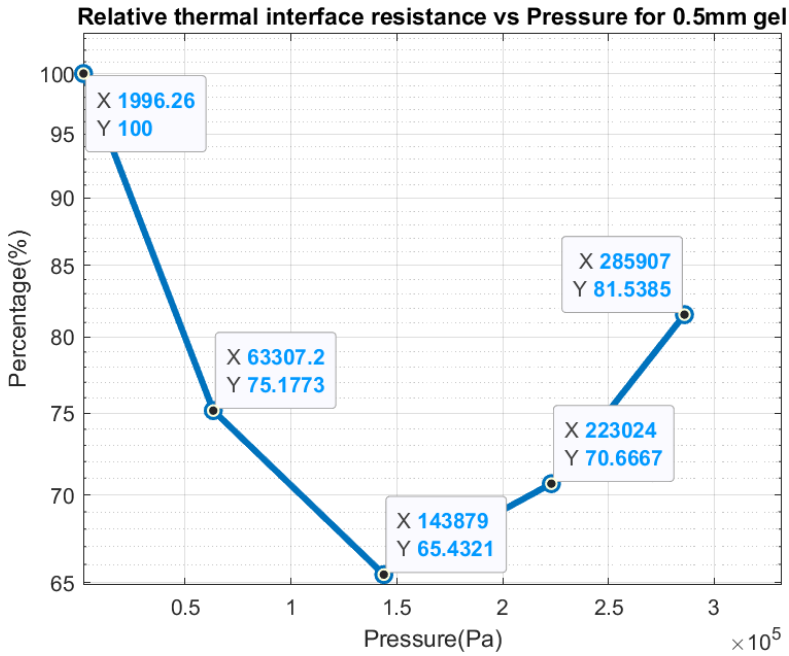

X- % change in Thermal Interface Resistance
Y- Pressure (Pa)
1 bar = 1 x 10^5 Pa

Figure 4.13: Percentage change in thermal interface resistance for 0.5mm thermal gel

5 Conclusion

The carbon footprint due to the transport sector has been on an all-time rise primarily due to the consumption of fossil fuels i.e., usage of internal combustion engines. To reduce the effect of burning fossil fuels, the transport sector came up with electric vehicles. These EVs use an all-electric and/or hybrid electric powertrain to drive the vehicle. The primary power source is the Li-ion battery that can generate enough power to drive the EV. To meet the space and weight requirements of EVs, these batteries are optimised to have high power and energy density. This optimization comes at the cost of maintaining the battery in its operating temperature range which is done by the BTMS. Out of the available BTMS's, the liquid cooling BTMS aided by a Thermal Interface Material proved to be effective out of the lot. This thesis conducted in collaboration with ESS Component Verification department at Volvo GTT aims to investigate the performance of commercially produced TIMs by varying the parameters like the thickness of TIMs and pressure applied on them.

Experimentation and simulation were preformed, with an understanding that one compliments another. In experimentation, two different TIM materials were placed between the battery and the coolant plate and these TIMs were tested and compared under different pressure conditions to analyse their thermal resistive properties. The temperature of the dummy cell vs pressure applied on the TIMs was plotted with the experimental data. To complement this, a parameter study was done with the help of simulation that aided us in extracting the values of thermal interface resistance of the TIM at the temperature conditions from experimentation. Then, thermal interface resistance at different pressures was plotted for both the TIMs and their behaviour was analyzed.

In the case of 2mm thermal pad of conductivity 3W/K.m the temperature of the cell was reduced by 5% over the range of pressure values, for the 2mm gel with conductivity 2.4W/K.m the temperature was reduced by 1.5% and for the 0.5mm thermal gel of similar conductivity the temperature initially reduced by 1.8% and then increased by 0.7%. To understand the behaviour of the TIMs the trend in thermal interface resistance is taken into consideration which shows that for the 2mm pad, there was a 40% reduction in the thermal interface resistance with an increase in pressure. Similarly, for the 2mm gel, there was 15% reduction in the same. But for the 0.5mm gel, the thermal interface resistance was reduced by 35% until the pressure increased to 1.4bar post which, it developed cracks on its surface due to which air bubbles were formed and the resistance increased by 16% at a pressure of 2.8bar.

6 References

[1] A. Kong, M. Zheng and X. Zhang, November 2021. [Online]. Available: https://www.greenpeace.org/static/planet4-eastasia-stateless/2021/11/47de8bb4-gpea_auto_environmental_guide_2021.pdf.

[2] R. Chinoracky, N. Stalmasekova and T. Corejova, "Trends in the Field of Electromobility—From the Perspective of Market Characteristics and Value-Added Services: Literature Review," *Energies,* vol. 15, no. 17, p. 6144, 2022.

[3] E. Gümüşsu, ÖEkici and M. Köksal, "3-D CFD modeling and experimental testing of thermal behavior of a Li-Ion battery," *Applied Thermal Engineering,* vol. 120, pp. 484-495, 2017.

[4] C. Bibin, M. Vijayaram, V. Suriya, R. S. Ganesh and S. Soundarraj, "A review on thermal issues in Li-ion battery and recent advancements in battery thermal management system," *Materials Today: Proceedings,* vol. 33, pp. 116-128, 2020.

[5] H. Liu, Z. Wei, W. He and J. Zhao, "Thermal issues about Li-ion batteries and recent progress in battery thermal management systems: A review," *Energy Conversion and Management,* vol. 150, pp. 304-330, 2017.

[6] S. Mohan, Y. Kim, J. Siegel, N. Samad and A. Stefanopoulou, "A Phenomenological Model of Bulk Force in a Li-Ion Battery Pack and Its Application to State of Charge Estimation," *Journal of The Electrochemical Society,* vol. 161, no. 4, pp. A2222-A22231, 2014.

[7] H. Berg, "Battery control and management," in *Batteries for Electric Vehicles*, 2015, pp. 168-193.

[8] Xia, Liu, Huang, Yang, Lai, Zheng, Wang, Wang and Wang, "Thermal Analysis and Improvements of the Power Battery Pack with Liquid Cooling for Electric Vehicles," *Energies,* vol. 12, no. 16, p. 3045, 2019.

[9] Park and Heesung, "A design of air flow configuration for cooling lithium ion battery in hybrid electric vehicles," *Journal of Power Sources,* vol. 239, pp. 30-36, 2013.

[10] Pesaran and A. A, "Battery thermal models for hybrid vehicle simulations," *Journal of Power Sources,* vol. 110, no. 2, pp. 377-382, 2002.

[11] X. Xu and R. He, "Research on the heat dissipation performance of battery pack based on forced air cooling," *Journal of Power Sources,* vol. 240, pp. 33-41, 2013.

[12] Y. W. J. Z. Zhongming Liu, "Shortcut computation for the thermal management of a large air-cooled battery pack," *Applied Thermal Engineering,* vol. 66, no. 2, pp. 445-452, 2014.

[13] K. Kelly, M. Mihalic and Z. M, "Battery usage and thermal performance of the Toyota Prius and Honda Insight during chassis dynamometer testing," in *Seventeenth Annual Battery Conference on Applications and Advances. Proceedings of Conference (Cat. No.02TH8576)*.

[14] R. Liu, J. Chen and J. Xun, "Numerical investigation of thermal behaviors in lithium-ion battery stack discharge," *Applied Energy,* pp. 288-297, 2014.

[15] T. L. Bergman, A. S. Lavine and F. P, Incropera's Principles of Heat and Mass Transfer, New York: John Wiley & Sons Inc, 2017.

[16] S. Basu, K. Hariharan, S. Kolake, T. Song, D. Sohn and T. Yeo, "Coupled electrochemical thermal modelling of a novel Li-ion battery pack thermal management system," *Applied Energy,* vol. 181, pp. 1-13, 2016.

[17] C. Lin, C. Cui and X. Xu, "Lithium-ion Battery Electro-thermal Model and Its Application in the Numerical Simulation of Short Circuit Experiment," *World Electric Vehicle Journal,* vol. 6, no. 3, pp. 603-610, 2013.

[18] A. Karimi and G. Dehghan, "Thermal Management Analysis of a Lithium-Ion Battery Pack using Flow Network Approach," *International Journal of Mechanical Engineering and Mechatronics,* 2012.

[19] S. Yang, C. Ling and Y. Fan, "A review of lithium-ion battery thermal management system strategies and the evaluate criteria," 2019.

[20] S. Yang, "A Review of Lithium-Ion Battery Thermal Management System Strategies and the Evaluate Criteria," *International Journal of Electrochemical Science,* pp. 6077-6107, 2019.

[21] W. Li, X. Zhuang and X. Xu, "Numerical study of a novel battery thermal management system for a prismatic Li-ion battery module," *Energy Procedia,* vol. 158, pp. 4441-4446, 2019.

[22] Z. Wang, X. Li, G. Zhang, Y. Lv, C. Wang, F. He and C. Yang, "Thermal management investigation for lithium-ion battery module with different phase change materials".

[23] Z. Qian, Y. Li and Z. Rao, "Thermal performance of lithium-ion battery thermal management system by using mini-channel cooling," *Energy Conversion and Management,* vol. 126, pp. 622-631, 2016.

[24] G. Pulugundla, P. Dubey and A. Srouji, "Time-accurate CFD analysis of liquid cold plates for efficient thermal performance of electric vehicle Li-ion battery modules," *SAE Technical Papers,* pp. 1-8, 2019.

[25] T. Han, B. Khalighi and S. Kaushik, "Li-ion Battery Thermal Management – Air vs. Liquid Cooling," in *Proceeding of Second Thermal and Fluids Engineering Conference*, 2017.

[26] J. Lazrak, A. Fourmigué and J. Robin, "An innovative practical battery thermal management system based on phase change materials: Numerical and experimental investigations," *Applied Thermal Engineering,* vol. 128, pp. 20-32, 2018.

[27] Z. Ling, F. Wang, X. Fang, X. Gao and Z. Zhang, "A hybrid thermal management system for lithium ion batteries combining phase change materials with forced-air cooling," *Applied Energy,* vol. 148, pp. 403-409, 2015.

[28] S. Bandhauer and T. Garimella, "Passive, internal thermal management system for batteries using microscale liquid–vapor phase change," *Applied Thermal Engineering,* vol. 61, no. 2, pp. 756-769, 2013.

[29] H. Hirano, T. Tajima, T. Hasegawa, T. Sekiguchi and M. Uchino, "Boiling Liquid Battery Cooling for Electric Vehicle," in *2014 IEEE Conference and Expo Transportation Electrification Asia-Pacific (ITEC Asia-Pacific)*, 2014.

[30] X. Xu, T. Xiao, S. Chen and S. Lin, "Exploring the heat transfer performance of nanofluid as a coolant for power battery pack," *Heat Transfer-Asian Research,* vol. 48, no. 7, pp. 2974-2988, 2019.

[31] R. Sabbah, R. Kizilel, J. Selman and S. Al-Hallaj, "Active (air-cooled) vs.

passive (phase change material) thermal management of high power lithium-ion packs: Limitation of temperature rise and uniformity of temperature distribution," *Journal of Power Sources,* vol. 182, no. 2, pp. 630-638, 2008.

[32] J. Hansson, T. Nilsson, L. Ye and J. Liu, "Novel nanostructured thermal interface materials: a review," *International Materials Reviews,* vol. 63, no. 1, pp. 22-45, 2018.

[33] D. Blazej, "Thermal Interface Materials," *Electronics Cooling,* vol. 9, no. 4, pp. 14-20, 2003.

[34] T. Ram and T. Abhay, "Thermal Performance Challenges from Silicon to Systems," p. 4, 2001.

[35] J. Ziemski and P. Khatri , ""Dry-to-the-touch" thermal grease," in *Proceedings International Symposium on Advanced Packaging Materials Processes, Properties and Interfaces (IEEE Cat. No.01TH8562)*.

[36] Y. Xian, P. Zhang, S. Zhai, P. Yuan and D. Yang, "Experimental characterization methods for thermal contact resistance: A review," *Applied Thermal Engineering,* vol. 130, pp. 1530-1548, 2018.

[37] S. R, M. D, Wunderle, B. Wittler, O. Gollhardt, A. Michel and B. R. H, "Characterization of thermal interface materials to support thermal simulation," *arXiv preprint arXiv:0709.1849,* 2007.

[38] Bosch, E. G. T, Lasance and C. J. M, "High accuracy thermal interface resistance measurement using a transient method," *Electronics Cooling,* vol. 6, pp. 26-33, 2000.

[39] M. L. Williamson, "Effect of surface deformations on contact conductance," 1992.

[40] Cooper, M. G, M. B. B and Y. M. M, "Thermal contact conductance," *International Journal of heat and mass transfer,* vol. 12, no. 3, pp. 279-300, 1969.

[41] M. Yovanovich, J. DeVaal and A. Hegazy, "Astatistical model to predict thermal gap conductance between conforming rough surfaces," in *3rd Joint Thermophysics, Fluids, Plasma and Heat Transfer Conference*, 1982.

DEPARTMENT OF MECHANICS AND MARITIME SCIENCES
CHALMERS UNIVERSITY OF TECHNOLOGY
Gothenburg, Sweden 2023
www.chalmers.se

CHALMERS
UNIVERSITY OF TECHNOLOGY